Journal of Asian Earth Sciences 79 (2014) 191–205

Contents lists available at ScienceDirect

Journal of Asian Earth Sciences

journal homepage: www.elsevier.com/locate/jseaes

Chemical heterogeneity of the Emeishan mantle plume: Evidence from highly siderophile element abundances in picrites

Jie Li [a], Xuan-Ce Wang [b,*], Zhong-Yuan Ren [a], Ji-Feng Xu [a], Bin He [a], Yi-Gang Xu [a]

[a] State Key Laboratory of Isotope Geochemistry, Guangzhou Institute of Geochemistry, Chinese Academy of Sciences, Guangzhou 510640, PR China
[b] ARC Center of Excellence for Core to Crust Fluid Systems (CCFS) and The Institute for Geoscience Research (TIGeR), Department of Applied Geology, Curtin University, Perth, WA 6845, Australia

ARTICLE INFO

Article history:
Received 1 July 2012
Received in revised form 22 August 2013
Accepted 6 September 2013
Available online 19 September 2013

Keywords:
Emeishan large igneous province
Picrite
Highly siderophile elements
Primary melt
Mantle plume
Chemical heterogeneity

ABSTRACT

Highly magnesian lavas or picrites have the potential to preserve important information about the origin and thermochemical state of the mantle source(s) of large igneous provinces. We have conducted a comprehensive study of highly siderophile element (HSE) concentrations in picrites from the ca. 260 Ma Emeishan large igneous province. We show that HSE abundances in the Emeishan picrites are greater than those in mid-ocean ridge basalts (MORBs) and parental melts of Hawaiian picrites, but are similar to those in komatiites. The picrites have two types of C1-normalized HSE patterns: (a) type 1, as represented by the Muli picrites is similar to that of the primitive upper mantle; (b) type 2, as represented by the Dali picrites resembles East Greenland and Iceland picrites. Pt/Ir and Pd/Ir ratios in the type 2 picrites are higher than those in type 1 picrites. The primary melt compositions of the studied samples have been estimated by back-addition of equilibrium olivine. The calculated HSE abundances of the parental liquids of the Dali and Muli picrites are higher than those of the parental melts to Hawaiian picrites. Along with previously published isotopic data, our study provides further evidence for chemical heterogeneity of the Emeishan mantle plume.

1. Introduction

Continental flood basalts (CFBs) are produced during short-lived and highly productive magmatic events and are characterized by basalts derived, in part, from an anomalously hot and enriched mantle reservoir (Bryan and Ernst, 2008; Coffin and Eldholm, 1992; Campbell and Griffiths, 1990; Richards et al., 1989). Although the mantle plume model has become a 'paradigm' for understanding the formation of CFBs over past three decades, other mechanisms have also been proposed for the formation of CFBs that do not invoke the presence of mantle plumes (Anderson and Natland, 2005; Foulger et al., 2005; McHone, 2000). Plumes are thought to be generated through heat transfer across the core-mantle boundary, which causes a thermal instability resulting in diapiric ascent of a large buoyant mass of hot mantle material (Campbell, 2007; Campbell and Griffiths, 1990). CFBs may provide a window into the deep Earth that can reveal the chemical and physical properties of the mantle plumes. However, the chemical and isotopic signatures of mantle plumes are difficult to identify, due to the magmas assimilating materials from the lithospheric mantle, continental crust, and volcanic edifices along with the superimposed effects of fractional crystallization. Highly magnesian lavas are generally a minor component of CFBs, but perhaps provide the most important information about the primary melts of CFB provinces (Herzberg and Gazel, 2009; Putirka et al., 2007).

The geochemistry of continental flood basalts in the Emeishan large igneous province (ELIP) has been interpreted as resulting from complex interactions between a mantle plume and heated lithospheric and asthenospheric mantle (Ali et al., 2005; Chung and Jahn, 1995; Hanski et al., 2004, 2010; Li et al., 2010; Song et al., 2008; Xu et al., 2001, 2004; Zhang et al., 2008, 2009). Although the Emeishan basalts are generally considered to be related to a mantle plume, the origin and chemical structure of the Emeishan plume is still a matter of debate. Some studies have suggested that the Emeishan mantle plume originated at the core-mantle boundary (CMB) as in the case of the Siberian CFBs (e.g., Li et al., 2010; Hanski et al., 2004; Lo et al., 2002). However, others studies consider that the Emeishan mantle plume originated from the upper–lower mantle boundary (e.g., Zhang et al., 2008). Abundances of highly siderophile elements (HSEs) are useful for characterizing the geochemical history of mantle reservoirs (e.g., Chazey Iii and Neal, 2005; Dale et al., 2008; Ireland et al., 2009; Jamais et al., 2008; Maier et al., 2009; Puchtel and Humayun, 2001). The siderophile and chalcophile nature of HSE, including the platinum-group elements (PGEs), indicates that they should be

* Corresponding author. Address: Department of Applied Geology, Curtin University, GPO Box U1987, Perth, WA 6845, Australia. Tel.: +61 8 9266 2453; fax: +61 8 9266 3153.
E-mail address: X.Wang3@curtin.edu.au (X.-C. Wang).

1367-9120/$ - see front matter © 2013 Elsevier Ltd. All rights reserved.
http://dx.doi.org/10.1016/j.jseaes.2013.09.009

highly enriched in Earth's core and significantly depleted in the mantle (e.g., Barnes et al., 1985; Walker, 2000). Thus, integrated studies of HSE abundances and Re-Os isotopes can potentially reveal the effect of core–mantle interaction on the chemical heterogeneity of mantle plume (e.g., Brandon et al., 1999; Brandon and Walker, 2005; Ireland et al., 2011; Walker et al., 1995).

The absolute and relative abundances of HSE have been determined in a number of previous studies measured HSE abundances in evolved lavas with MgO < 7% and proposed that the observed fractionations of HSE resulted from the crystallization of olivine, chromite and a trace alloy with the latter being incorporated in olivine and/or chromite (Li et al., 2012; Qi and Zhou, 2008; Wang et al., 2007a, 2011). Based on a small dataset, Wang et al. (2007a) suggested that the diversity of HSE geochemistry in Emeishan CFBs was produced by crustal contamination. Wang et al. (2011) determined HSE concentration in a suite of intrusive rocks and low-magnesian lavas, and concluded that fractionation crystallization under either sulfur-undersaturated or sulfur-saturated conditions controlled the HSE behavior. However, there have been few systematic studies of the HSE in highly magnesian lavas from the ELIP (i.e., MgO > 12 wt.%; Li et al., 2012).

To better understand the HSE systematics of the ELIP parental melts, we collected picrites (MgO > 12 wt.%) and related tholeiitic basalts (MgO = 9–11 wt.%) from in the eastern part of the ELIP (Fig. 1). Compared with less primitive basalts, these highly magnesian lavas have the potential to provide more direct information about the thermochemical state of their source mantle (Herzberg et al., 2007; Herzberg and Gazel, 2009; Putirka, 2005; Wang et al., 2007b, 2012). As such, these primitive picrites and basalts may be particularly useful in constraining the HSE content of the mantle source of the Emeishan mantle plume, which is the primary objective of our study.

2. Geological setting and samples

The ELIP forms a massive Permian–Triassic succession of volcanic rocks along the western margin of the Yangtze Craton (Ali et al., 2005; Chung et al., 1995; Xu et al., 2001, 2004; He et al., 2003). These volcanic rocks cover an area of >2.5 × 10^5 km^2, with a diameter of ~500 km (Chung and Jahn, 1995; Xu et al., 2004; Ali et al., 2005). The ELIP comprises a succession of tholeiites, with minor picritic and rhyolitic/trachytic lava flows. In addition to the extrusive rocks, mafic–ultramafic layered complexes, dikes, sills, and syenitic and other alkaline intrusions form part of the ELIP. Prior to the eruption of the ELIP, He et al. (2003) argued that large-scale lithospheric uplift occurred in the region, although this point is disputed by Utskins-Peate and Bryan (2008) and Sun et al. (2010). The ELIP was formed during the Late Permian, but differing views still exist on the exact timing of the volcanism and its potential relationship to mass extinction events. SHRIMP zircon U–Pb dating of mafic intrusions, dikes, and volcanic rocks has produced ages of 257–263 Ma (Zhong and Zhu, 2006; He et al., 2007; Zhou

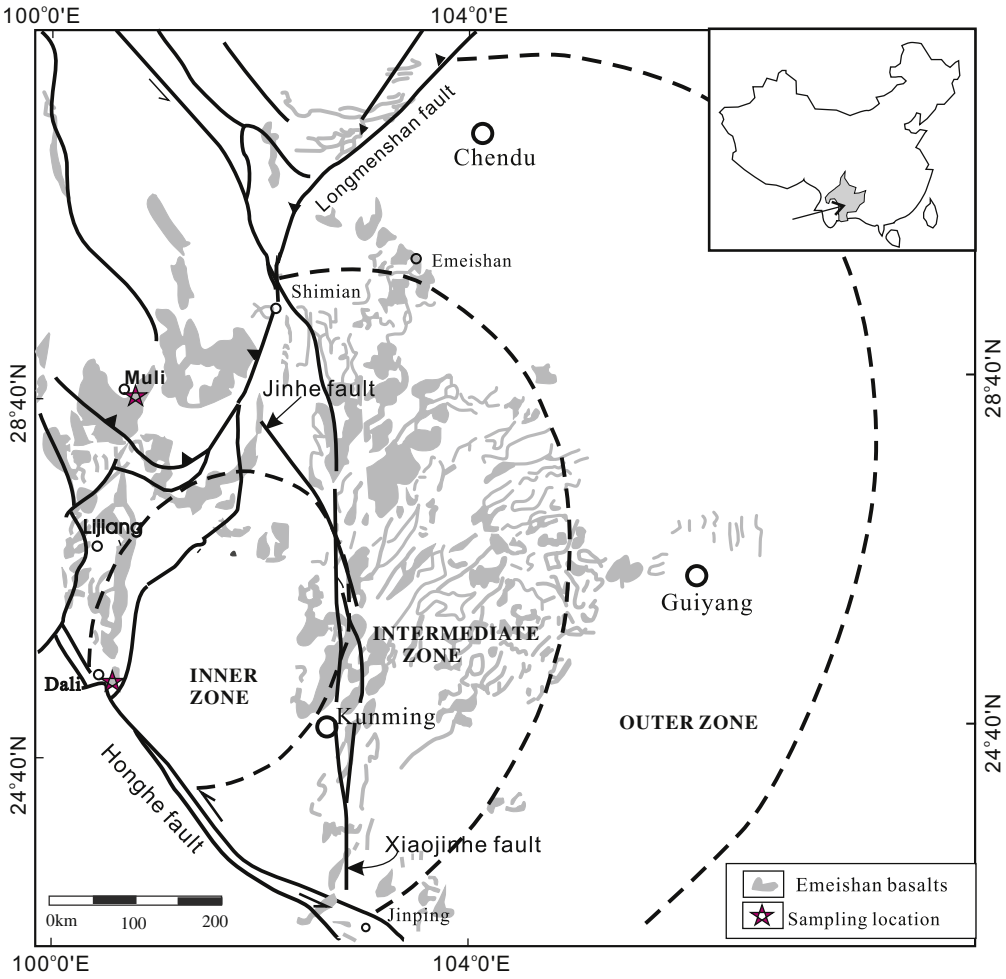

Fig. 1. Schematic illustration of the geological features of the Emeishan large igneous province, also showing sample locations (modified after Xu et al., 2004).

et al., 2002, 2008; Fan et al., 2008; Shellnutt and Jahn, 2011), whereas $^{40}Ar/^{39}Ar$ dating of volcanic and intrusive rocks has yielded ages of 254 ± 5 Ma (Boven et al., 2002) and 251–253 Ma (Lo et al., 2002). More precise zircon U–Pb age determinations of mafic and silicic intrusive rocks from the ELIP have yielded a narrow range of ages between 257 Ma and 260 Ma (Shellnutt et al., 2012). Consequently, it is now accepted that the Emeishan CFBs were erupted at ca. 260 Ma.

The samples analyzed in this study were collected from the Dali and Muli areas (Fig. 1). Details about the samples, including their specific locations and whole-rock geochemistry, have been published elsewhere (Xu et al., 2001; Li et al., 2010; Hanski et al., 2010). The picrites from the Muli area are strongly altered and, apart from a few fresh clinopyroxene crystals, all primary magmatic minerals have been replaced by serpentine, talc, and chlorite. Fresh olivine has not been found in these rocks, but the presence of olivine pseudomorphs indicates that olivine was abundant when the picrites were erupted. Fresh diopsidic clinopyroxene is present either as phenocrysts or in the matrix. Most of the Dali picrites are highly porphyritic (>25 vol.% phenocrysts) and contain abundant phenocrysts of forsteritic olivine, along with minor amounts of clinopyroxene ± orthopyroxene. Olivine phenocrysts are generally subhedral to rounded, occasionally embayed or partly resorbed, and are partially serpentinized along grain cracks and margins. Some olivine crystals host equant, euhedral to rounded Cr-spinel crystals that are a few tens of microns in diameter. Cr-spinel is also present as isolated grains in the groundmass. The groundmass consists principally of very fine-grained, intergrown clinopyroxene and plagioclase, as well as some devitrified glass.

3. Analytical techniques

For major and trace element analyses, volcanic rock samples were first split into small chips, and then soaked in 2 N hydrochloric acid for 1 h to remove alteration minerals. The rock chips were then powdered in an alumina ceramic shatter box. Major elements were determined by X-ray fluorescence (XRF) spectrometry on fused glass disks, whereas trace element were measured with a Perkin Elmer Elan 6000 inductively coupled plasma-mass spectrometer (ICP–MS) at the Guangzhou Institute of Geochemistry, Chinese Academy of Science (GIG-CAS). Analytical uncertainties are ±1–2% for major elements, ±5% for rare-earth elements, ±5–10% for other trace elements. Full details of the analytical procedures are described by Chen et al., 2010.

For PGE and rhenium concentration measurements, rock samples were first split into small chips using a hammer wrapped in paper to avoid contamination. All PGE abundances were determined by isotope dilution techniques. Approximately 2 g of whole rock powder was combined with a mixed PGE spike (^{190}Os, ^{191}Ir, ^{99}Ru, ^{194}Pt, ^{105}Pd and ^{185}Re) and attacked for 24 h at 240 °C in Carius tubes with reverse aqua regia (3 ml concentrated HCl + 9 ml concentrated HNO_3) (Shirey and Walker, 1995). Osmium was extracted from the Re- and PGE-bearing solution as OsO_4 into carbon-tetrachloride (CCl_4) and back-extracted into HBr (Cohen and Waters, 1996). Final purification of the Os was achieved by micro-distillation. Osmium abundances were measured using a Thermo-Finnigan TRITON® thermal ionization mass spectrometer (TIMS) in negative ion detection mode (Creaser et al., 1991; Volkening et al., 1991) at GIG-CAS.

Rhenium, Ir, Ru, Pt, and Pd were separated from aqua regia by cation exchange chromatography using pre-cleaned Bio-Rad AG 50W-X8 resin (100–200 mesh). To eliminate Cr-based polyatomic interferences on ^{101}Ru, which may result in erroneously elevated Ru abundances if measurements are performed by ICP-MS (Meisel et al., 2008), 1 mL of 30% H_2O_2 was added to reduce Cr (VI) to Cr (III) before loading onto the cation exchange column. Rhenium, Ir, Ru, Pt and Pd were eluted with 30 mL of 0.5 N HCl. However, the PGE fractions after cation exchange chemistry still contain significant amounts of impurities such as Mo, Zr and Hf whose oxide species can interfere on PGE masses. As such, a clean-up procedure using Amberchrom CG-71m resin coated with N-benzoyl-N-phenylhydroxylamine (BPHA) was carried out to eliminate Mo, Zr and Hf (Li et al., in press). Rhenium, Ir, Ru, Pt and Pd are not absorbed onto the resin and were eluted with 7 mL of 0.5 N HCl into the same fraction. The eluted solution was evaporated to near dryness and dissolved in 0.3 N HNO_3 for ICP-MS analysis.

Rhenium, Ir, Ru, Pd and Pt abundances were measured by isotope dilution on a Thermo-Scientific XSERIES-2 ICP-MS. The sample was introduced to the plasma with a conventional Scott-type glass spray chamber. We measured the following isotope masses for PGE and Re concentration calculations: ^{99}Ru, ^{100}Ru, ^{101}Ru, ^{105}Pd, ^{106}Pd, ^{108}Pd, ^{185}Re, ^{187}Re, ^{191}Ir, ^{193}Ir, ^{194}Pt, and ^{195}Pt. Isotope masses of ^{90}Zr, ^{95}Mo, ^{111}Cd, ^{178}Hf and ^{192}Os were also monitored to allow isobaric interference corrections to be made where necessary. Interference corrections were typically negligible, and only an ^{106}Cd interferences on ^{106}Pd was significant (ca, 5% correction) in some samples. Oxide formation (CeO^+/Ce^+) was minimized by tuning to $\leqslant$1.5%. Instrumental mass fractionation was determined and corrected for by bracketing analyses of a 2 ng/g of PGE standard solution. The Pt blank over the period of this study ranged from 25 to 40 pg. Other PGE and Re blanks are generally $\leqslant$10 pg. All the presented concentration data have been blank corrected. The blank contributions to measured PGE contents were <2% for all samples, and for Re contents were <10% for most samples.

Analytical results for standard reference materials, including BHVO-2 (basalt) and WPR-1 (peridotite) are presented in Table 1. The standard PGE and Re concentration data obtained here show good agreement with those reported by Meisel and Moser (2004). The poorer reproducibilities of PGE concentrations in BHVO-2 may reflect sample heterogeneity (i.e., the "nuggets effect").

4. Results

Major and trace element data and HSE concentrations for picrites and related basalts are presented in Tables 2 and 3. Picrites from the Muli and Dali area are characterized by high MgO (>12 wt.%), Mg# (Mg# = Mg/[Mg + Fe^{2+}]; Mg# > 71; assuming

Table 1
Analytical data (in ng/g) for reference materials BHVO-2 (basalt) and WPR-1 (peridotite).

	BHVO-2			WPR-1		
	Average (N = 6)	RSD (%)	Meisel and Moser, 2004	Average (N = 6)	RSD (%)	Meisel and Moser, 2004
Pt	8.56	24	10.1	296	8	298
Pd	3.14	13	2.94	256	6	258
Re	0.549	3	0.543	10.7	6	10.83
Os	0.083	13	0.101	17.18	10	18.55
Ru	0.139	16	0.129	22.95	4	22.8
Ir	0.06	21	0.058	15.19	15	16.7

Table 2
Major and trace element concentrations of picrites from the Muli and Dali areas (ML = Muli area; RX and DL = Dali area).

Samples	SiO_2	TiO_2	Al_2O_3	$Fe_2O_3^T$	MnO	MgO	CaO	Na_2O	K_2O	P_2O_5	LOI	Al_2O_3/TiO_2	Mg#	Cr	Ni	Nb	La	Yb	La/Yb
	Weight percent													Parts per million					
ML-32	37.8	1.6	10.8	14.3	0.2	22.0	7.7	<0.01	<0.01	0.1	7.1	6.8	78	1238	750	8.1	9.6	1.5	6.3
ML04-17	37.7	1.0	8.4	11.9	0.2	17.9	13.3	0.6	0.1	0.1	9.1	8.4	78	1648	953	4.9	11.6	1.1	10.9
ML04-33	44.9	1.3	7.3	11.5	0.2	21.0	9.3	0.2	0.0	0.0	4.1	5.6	81	1687	1008	7.1	9.4	1.2	7.9
ML-23	45.4	1.8	13.0	13.0	0.2	11.8	7.5	3.1	<0.01	0.1	4.1	7.2	68	904	407	6.0	6.8	1.8	3.8
ML04-49	47.9	1.1	11.1	13.5	0.2	13.3	6.0	2.9	0.1	0.0	3.8	10.1	70	610	320	7.3	17.1	1.7	10.2
ML04-18	40.6	1.2	8.8	13.7	0.2	19.9	9.6	0.4	0.0	0.1	5.8	7.3	77	2062	1327	5.4	1.9	1.1	1.7
ML04-19	41.6	1.1	8.8	12.6	0.2	21.2	8.8	0.5	0.0	0.1	5.3	8.0	80	1429	830	3.1	1.5	1.3	1.2
ML04-23	50.0	1.6	11.5	10.7	0.1	12.7	6.0	3.7	0.1	0.2	3.3	7.2	74	892	527	6.4	3.5	1.4	2.4
ML-28	40.2	1.7	10.6	14.2	0.2	16.6	10.4	0.7	<0.01	0.1	5.7	6.2	73	1640	661	6.6	7.6	1.3	5.7
ML04-20	41.8	1.6	8.9	13.8	0.2	18.8	10.1	0.3	0.0	0.2	4.5	5.6	76	2570	832	6.0	9.1	1.4	6.5
ML04-45	40.7	1.6	10.4	14.7	0.2	18.9	7.0	0.5	0.1	0.1	5.2	8.5	75	2012	1143	8.6	8.6	1.4	6.0
ML04-44	48.7	2.2	13.2	12.7	0.2	8.8	6.3	2.9	1.0	0.0	3.5	6.0	62	440	257	27.0	29.0	2.3	12.6
ML04-46	50.0	2.5	11.8	12.9	0.2	8.9	7.3	3.3	0.0	0.2	2.5	4.7	62	891	259	30.9	36.3	2.8	13.1
RX-1	41.6	2.0	7.2	12.8	0.2	20.2	9.0	0.3	0.0	0.2	6.7	3.6	79	2562	952	22.7	22.5	1.4	15.6
RX-2	41.0	1.6	8.1	12.8	0.2	20.1	8.9	0.3	0.2	0.2	6.9	5.1	79	2012	711	14.1	13.0	1.5	8.9
RX-3	40.8	1.7	8.6	13.4	0.2	19.3	8.7	0.3	0.5	0.2	6.6	5.1	77	1896	672	14.9	13.5	1.5	9.1
RX-4	41.0	1.6	8.2	12.7	0.2	20.3	8.7	0.3	0.2	0.2	7.0	5.1	79	2073	699	14.1	12.7	1.4	8.8
RX-5	40.6	1.6	7.8	12.6	0.2	20.4	8.9	0.2	0.1	0.2	7.7	4.9	79	1890	697	14.3	12.9	1.4	8.9
RX-7	41.9	1.6	7.9	12.4	0.2	20.0	8.6	0.2	0.2	0.2	7.0	4.9	79	1898	672	14.2	13.0	1.5	8.9
RX-8	49.4	1.9	12.3	9.9	0.1	10.5	6.6	2.5	2.8	0.2	3.8	6.5	71	424	217	24.0	22.0	1.8	12.3
RX-9	40.2	1.7	8.1	13.0	0.2	19.8	9.4	0.3	0.1	0.2	7.1	4.8	78	2009	722	15.4	13.9	1.5	9.2
RX-11	40.8	1.7	8.3	12.9	0.2	19.7	8.9	0.3	0.4	0.2	7.0	4.9	78	1852	686	14.9	13.0	1.5	8.9
RX-12	40.9	1.6	8.5	12.9	0.2	19.6	8.7	0.3	0.4	0.2	7.0	5.3	78	2004	664	14.5	13.0	1.4	9.1
DL08-3	43.9	0.9	8.1	11.6	0.2	21.6	8.3	0.9	0.5	0.1	3.8	9.0	81	2220	976	7.7	7.8	1.4	5.5
DL08-5	45.1	1.1	10.1	11.3	0.2	17.5	9.2	1.2	0.7	0.1	3.5	9.2	78	1977	725	9.0	9.0	1.6	5.5
DL08-6	44.7	1.1	9.3	11.7	0.2	18.0	9.2	1.1	0.7	0.2	3.7	8.5	78	1839	769	9.2	9.4	1.7	5.7
DL08-7	44.2	1.0	8.4	11.7	0.2	20.9	8.6	1.0	0.5	0.1	3.6	8.4	81	2252	945	8.3	8.3	1.5	5.5
DL08-8	44.6	1.1	9.4	11.7	0.2	17.9	9.2	1.0	0.7	0.1	4.1	8.5	78	1849	738	9.3	9.3	1.7	5.5
DL08-12	44.3	1.0	8.3	11.3	0.1	19.8	7.4	0.4	0.4	0.1	6.9	8.3	80	2207	936	8.0	8.2	1.5	5.4
DL08-13	44.5	1.0	8.5	11.5	0.2	20.2	8.1	0.9	0.5	0.1	4.4	8.5	80	2198	919	8.1	8.2	1.5	5.5
DL08-15	45.1	1.1	9.3	10.9	0.1	18.5	8.1	0.6	0.6	0.1	5.6	8.5	80	2154	918	8.9	9.3	1.6	5.7
DL08-16	45.4	1.2	10.0	11.4	0.2	17.0	8.9	1.1	0.7	0.2	4.0	8.3	78	1971	712	9.9	9.9	1.8	5.6

Table 3
Highly siderophile element (HSE) concentrations of picrites from the Muli and Dali areas.

Samples	Os	Ir	Ru	Pt	Pd	Re	Total PGE	Pd/Ir	Pt/Ir	Pt/Os
Parts per billion										
ML-32	1.17	1.14	2.72	10.06	4.08	0.01	19.15	3.59	8.85	8.62
ML04-17	2.21	1.36	2.59	10.90	4.59	0.01	21.65	3.37	8.00	4.94
ML04-33	0.51	0.82	1.92	3.87	1.55	0.19	8.68	1.89	4.70	7.59
ML-23	1.35	0.79	1.16	12.02	3.18	0.08	18.50	4.01	15.19	8.88
ML04-49	1.38	0.27	0.88	2.65	1.57	0.03	6.75	5.85	9.89	1.92
ML04-18	2.56	1.97	2.89	8.67	4.46	0.14	20.56	2.27	4.41	3.38
ML04-19	1.46	1.61	2.67	12.30	9.15	0.01	27.19	5.70	7.66	8.41
ML04-23	0.88	1.16	1.62	11.17	4.90	0.02	19.74	4.23	9.63	12.67
ML-28	2.14	1.52	2.28	20.92	8.43	0.37	35.28	5.54	13.76	9.79
ML04-20	3.28	2.36	4.17	19.71	10.14	0.24	39.66	4.30	8.36	6.01
ML04-45	2.24	1.66	4.03	9.32	4.83	0.16	22.08	2.91	5.61	4.15
ML04-44	0.40	0.43	0.41	3.45	1.66	0.13	6.33	3.88	8.08	8.62
ML04-46	0.48	0.59	0.47	6.09	2.67	0.14	10.30	4.55	10.39	12.69
RX-1	1.93	1.96	2.56	17.44	2.45	0.12	26.34	1.25	8.91	9.05
RX-2	1.40	0.74	1.76	9.93	3.48	0.11	17.30	4.71	13.44	7.10
RX-3	0.97	0.97	1.79	8.62	3.65	0.06	15.99	3.77	8.92	8.90
RX-4	0.96	0.80	1.91	8.74	3.64	0.07	16.06	4.54	10.88	9.13
RX-5	1.18	0.92	2.02	8.92	3.12	0.08	16.16	3.41	9.73	7.56
RX-7	1.00	0.84	1.89	8.76	3.18	0.08	15.67	3.77	10.37	8.78
RX-8	0.48	0.21	0.57	4.61	1.78	0.06	7.65	8.37	21.71	9.64
RX-9	1.32	0.82	1.82	27.73	3.99	0.06	35.70	4.85	33.65	20.95
RX-11	1.02	1.04	2.02	12.81	3.89	0.07	20.78	3.74	12.31	12.57
RX-12	3.24	0.78	2.31	7.93	3.42	0.03	17.67	4.41	10.21	2.45
DL08-3	1.13	1.15	3.23	20.31	8.23	0.39	34.05	7.17	17.70	18.03
DL08-5	0.78	0.66	1.38	13.93	7.44	0.44	24.19	11.21	20.99	17.78
DL08-6	0.85	0.50	1.84	10.69	6.09	0.46	19.97	12.11	21.26	12.65
DL08-7	0.86	1.23	2.18	10.64	5.67	0.44	20.58	4.62	8.67	12.35
DL08-8	0.80	0.74	1.62	25.39	6.42	0.49	34.96	8.72	34.52	31.77
DL08-12	1.09	0.80	2.80	10.08	4.81	0.40	19.58	6.03	12.65	9.23
DL08-13	0.96	0.73	1.70	10.10	6.85	0.44	20.34	9.33	13.77	10.48
DL08-15	0.78	0.74	1.37	11.92	7.52	0.36	22.33	10.10	16.02	15.33
DL08-16	0.70	0.65	1.19	10.12	6.11	0.58	18.76	9.46	15.67	14.41

Fe^{2+} = 0.9 × total Fe), Cr (610–2570 ppm) and Ni (320–1327 ppm). This indicates that these picrites are primitive samples and may represent, or be almost, primary melts. In contrast, four basaltic samples have relatively low compatible elements contents (Table 2). The Muli picrites hvae a large range of La/Yb (1.2–10.9) and Al_2O_3/TiO_2 ratios (5.6–10.1), whereas with the exception of one sample (RX-1), the Dali picrites have almost constant La/Yb (5.4–5.7 for the DL suite and 8.9–9.2 for the RX suite) and Al_2O_3/TiO_2 ratios (8.3–9.2 for the DL suite and 4.8–5.3 for the RX suite).

The absolute HSE abundances in all the picrites are greater than those in MORB and in the parental magmas of Hawaiian picrites, but are similar to those in komatiites (Figs. 2 and 3). The concentrations of I-group PGEs (Os, Ir, and Ru = 0.2–2.4 ppb) in all samples are less than estimates for primitive upper mantle (e.g., Becker et al., 2006), whereas concentrations of p-group PGEs (Pd and Pt, Pt concentrations range from 2.6 to 27.8 ppb) are comparable to estimate for PUM. With the exception of Re, HSE concentrations in the Emeishan picrites are generally similar to the abundances reported for the picrites from Hawaiian, Iceland and East Greenland (Fig. 3).

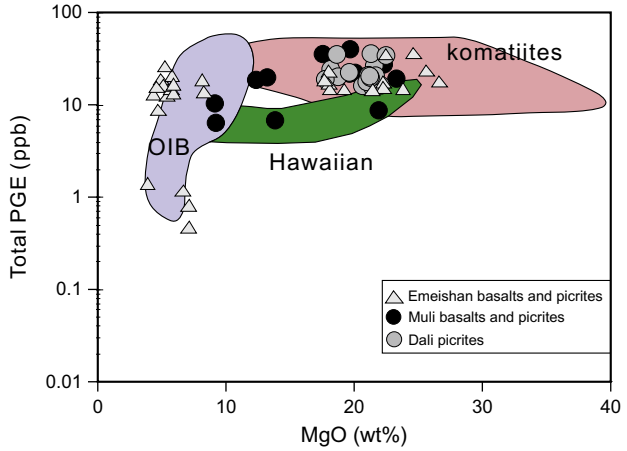

Fig. 2. Total PGE contents plotted versus MgO. The reference fields are from Ely and Neal (2003) and data for the Emeishan basalts and picrites are from Li et al. (2012).

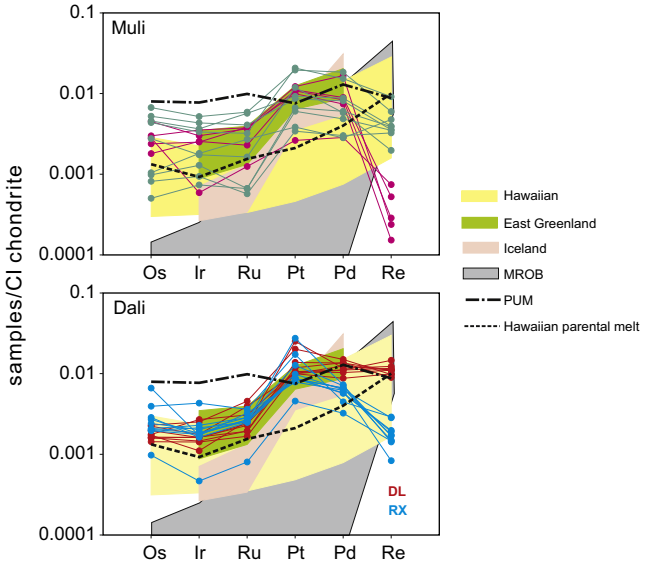

Fig. 3. CI-chondrite-normalized HSE patterns for (a) Muli and (b) Dali picrites. Primitive upper mantle (PUM) is considered to be representative of fertile peridotites prior to depletion of the upper mantle (Becker et al., 2006). The reference MORB field is modified after Dale et al. (2008). The primitive melt for Hawaiian picrites is an average of individual parental melts (Ireland et al., 2009). The chondrite normalizing values are from McDonough and Sun (1995). Data sources: east Greenland picrites – Momme et al. (1997, 2006); Iceland picrites – Momme et al. (2003); Hawaiian picrites – Bennett et al. (2000), Ireland et al. (2009), and Pitcher et al. (2009).

Chondrite-normalized HSE patterns of the Muli picrites are characterized by relatively uniform Pt/Ir (typically 7–10; average = 9.3 ± 4.2) and Pd/Ir (typically 1.9–5.9; average of 4.3 ± 1.9). These rocks can be divided into two sub-types in terms of Re abundances. One type is strongly depleted in Re, with concentrations that are significantly lower than those in MORB. The other type is slightly depleted in Re with abundances comparable to Hawaiian picrites and MORB (Fig. 3). HSE patterns are similar to picrites from East Greenland with consistent Os–Ir–Ru pattern, but higher Pt and Pd abundances as compared with Iceland picrites and MORB (Fig. 3). The Dali picrites are characterized by more fractionated Pt/Ir (8–33; average = 15.9 ± 8.4) and Pd/Ir (1.3–12.1; average = 6.6 ± 3.0) ratios than the Muli picrites.

When considering data for the entire picrite suite, Os, Ir, Ru, Pt and Pd are negatively correlated with SiO_2 and Al_2O_3 (Fig. 4). Osmium, Ir and Ru in the Muli picrites correlate positively with MgO (Fig. 5). Inflections appear at MgO contents of ca. 18 wt.% on plots of Os, Pt, Pd, and Re versus MgO (Fig. 5). At MgO contents <18 wt.%, Os, Pt, and Pd decrease with decreasing MgO, whereas at MgO contents >18 wt.%, these PGE increase with decreasing MgO. The Dali picrites exhibit a small range of MgO contents (17–23 wt.%) and display broad correlations on plots of Os-, Ir-, and Re versus MgO. PGE concentrations in the Muli picrites correlate strongly with Cr and Ni with inflections at Ni ≈ 700 ppm on the Ni-MgO trend (Figs. 5 and 6b). PGE contents of the Dali picrites are highly variable, and do not show systematic trend with MgO contents (Fig. 6).

5. Discussion

Highly siderophile elements in the Emeishan picrites exhibit a large range in absolute and relative abundances (Table 3 and Figs. 2 and 3). These variations can be attributed to several factors, including volatile losses in subaerial and shallow submarine flows (e.g., Ireland et al., 2009; Lassiter, 2003; Norman et al., 2004; Sun et al., 2003), crystal-liquid fractionation, and crustal contamination processes (AFC) (e.g., Righter et al., 2004; Dale et al., 2008; Jamais et al., 2008; Qi and Zhou, 2008; Ireland et al., 2009; Wang et al., 2011; Zhong et al., 2011). Volatile loss can affect abundances of Re and perhaps Ir. Prior to using the HSE to characterize the mantle source of the Emeishan picrites, these potential secondary effects need to be considered.

5.1. Estimation of parental melt compositions

Estimation of a parental melt composition is essential in trying to deconvolve the effects of crystal-liquid fractionation on HSE abundances. The parental melt represents the most primitive magma that was produced directly by melting of the mantle source. Samples that have major element compositions approaching the estimated parental melt compositions are presumed to have experienced olivine fractionation following separation from their mantle sources (e.g., Herzberg et al., 2007; Herzberg and Gazel, 2009; Putirka, 2005; 2007). Consequently, these samples best preserve the HSE composition of the parental melt. Samples that deviate from the parental melt composition have likely experienced variable amounts of crystal-liquid fractionation and/or crustal contamination.

Parental melt compositions of basaltic rocks can be estimated by addition or subtraction of equilibrium olivine back into or from

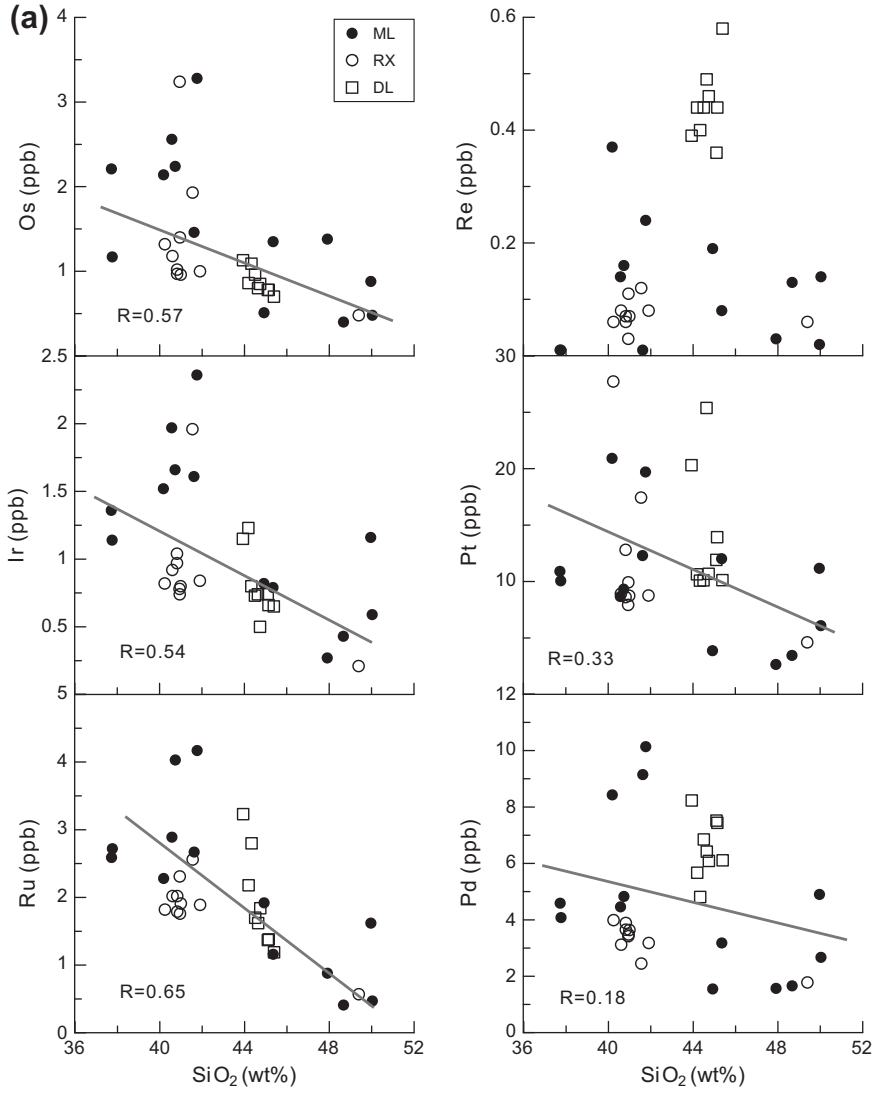

Fig. 4. PGE concentrations in the Muli and Dali picrites plotted versus (a) SiO_2 and (b) Al_2O_3. The dashed lines indicate the correlation between PGE contents and SiO_2 or Al_2O_3.

selected samples, that have experienced fractional crystallization or accumulation of only olivine (e.g., Danyushevsky et al., 2000; Putirka, 2005; Herzberg et al., 2007; Wang et al., 2012). Despite the fact that compatible element contents (e.g., MgO, Cr, and Ni) of the studied picrites are similar to those of melts derived directly from the mantle, the linear trends evident in Figs. 4–6 clearly show that variable proportions of olivine accumulation and removal have played an important role in the generation of these picrites. A series of olivine and basalt compositions were calculated from starting materials as follows: (1) the composition of equilibrium olivine was obtained using K_D $(Fe/Mg)^{oliv/liq} = 0.33$ (Putirka, 2005), assuming that $Fe^{2+}/(Fe^{2+} + Fe^{3+}) = 0.90$ in the melt (Frost and McCammon, 2008); (2) a more primitive basalt composition was calculated as a mixture of the basalt and equilibrium olivine in a weight ratio of 99.9:0.1; (3) steps (1) and (2) were repeated using the calculated primitive basalt to progressively obtain more primitive basalt compositions (Wang et al., 2012). The calculated of olivine and basalt compositions were repeated until the calculated equilibrium olivine had a forsterite content of Fo_{91}. Mg-rich olivine phenocrysts in the Lijiang (Zhang et al., 2006) and Dali picrites (Hanski et al., 2010) of the western Emeishan CFB province, have Fo values up to 91.6 and 93.5, respectively. To minimize the effects of clinopyroxene fractionation and alteration, only samples with MgO ⩾ 12 wt.%, CaO > 9 wt.%, SiO_2 ⩾ 44 wt.% and loss on ignition <5 wt.% were chosen as starting materials. Six samples (ML-04-33 and DL08-5, -6, -7,-8, and -16) were chosen as starting materials to these calculations the parental melts. The estimated arental melts have 47–48 wt.% SiO_2, 17–19 wt.% MgO, 8.5–11 wt.% Al_2O_3, 9.0–10.5 wt.% FeO, and 9–11 wt.% CaO (Table 4). The uncertainties are mainly due to the variability of K_D $(Fe/Mg)^{oliv/liq}$ and Fe^{2+}/Fe^{total} (Putirka, 2005), which will result in uncertainties ca. 3% for MgO and ca. 1% for SiO_2, Al_2O_3 and CaO. Variability in the compositions of high-Mg olivine phenocrysts (Fo > 90) may also contribute to the uncertainties. Even considering these uncertainties, our estimates likely represent the minimum values of the major element compositions of the primary melts.

5.2. Effects of volatile loss and alteration on PGE and Re abundances

Volatile loss has been demonstrated to play an important role in the Re depletion of basaltic rocks (Sun et al., 2003; Lassiter, 2003; Norman et al., 2004). This effect may cause fractionation of Re from the other HSE. The potential for Re loss is consistent with petrographic evidence that shows the Muli picrites are highly altered,

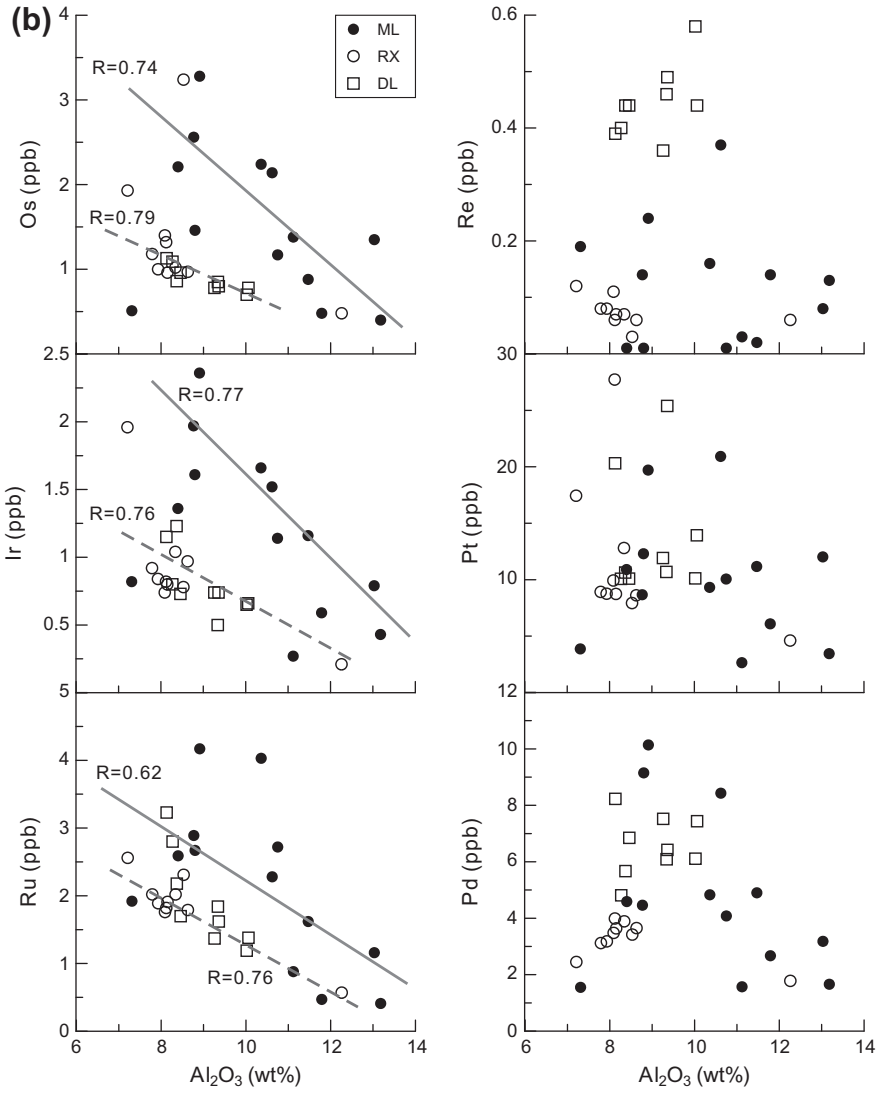

Fig. 4 (*continued*)

but relatively less so in the case of the Dali picrites. In general, chondrite-normalized HSE patterns for picritic suites show marked Re enrichments (Ireland et al., 2009). However, in the Muli lavas that were erupted in a subaqueous or in a shallow marine environment, chondrite-normalized HSE patterns show relative depletions of Re, which is consistent with Re loss from the lava flows. Five Muli picrites (ML-32, ML04-17, ML04-19, ML-04-23, and ML-04-49) have chondrite normalized Re values of <0.001 and show a strong depletions in Re on chondrite-normalized HSE patterns (Fig. 3). The DL picrites with flat Pt–Pd–Re patterns do not show such obvious depletions in Re abundances, although these can be observed in RX samples (Fig. 3).

Good correlations between an immobile element and another selected element can be taken as evidence of immobile element behavior (Polat and Hofmann, 2003). Aluminum (Al) is the most immobile element during low-temperature alteration of highly magnesian lavas (i.e., Komatiites, P131-148). As shown in Fig. 4, but with the exception of samples RX-12, ML04-33, and ML04-49, all samples show good correlations between PGE concentrations and Al_2O_3 contents. This suggests that all the PGE (apart from Re) have essentially been immobile during low-temperature alteration. Although the samples have a large range in PGE abundances, all the studied samples show uniform chondrite normalized patterns (with the exception of Re). This provides further evidence for the immobility of most PGE elements in our studied picrites. In contrast, there is no meaningful correlation between Re and Al_2O_3 (Fig. 4), which suggests Re was mobile during alteration.

5.3. HSE characteristics of the parental melts

Given the linear trends evident in Figs. 4–6, the removal and accumulation of olivine can be assumed to have had a major effect on the absolute and relative HSE abundances in the studied picrites. This may be attributable to the co-precipitation of phases such as PGE alloys with the olivine phenocrysts (Ireland et al., 2009 and references therein). Combining the linear trend of HSE versus MgO and the estimated primary MgO contents can provide first-order constraints on the HSE composition of the parental melts for each picritic suite (Fig. 7). Osmium, Ir, and Ru contents of the Muli parental melt were estimated using this method to be: Os = 2.59 ± 0.30 ppb, Ir = 1.84 ± 0.45 ppb and Ru = 3.00 ± 0.69 ppb (all 2 SD). Platinum and Pd exhibit more a complex behavior and the estimates for Pt (16 ± 4 ppb) and Pd (10 ± 4 ppb) contents in the parental melts are based on the positive linear correlations defined by samples with MgO < 20 wt.%. The Muli picrites do not

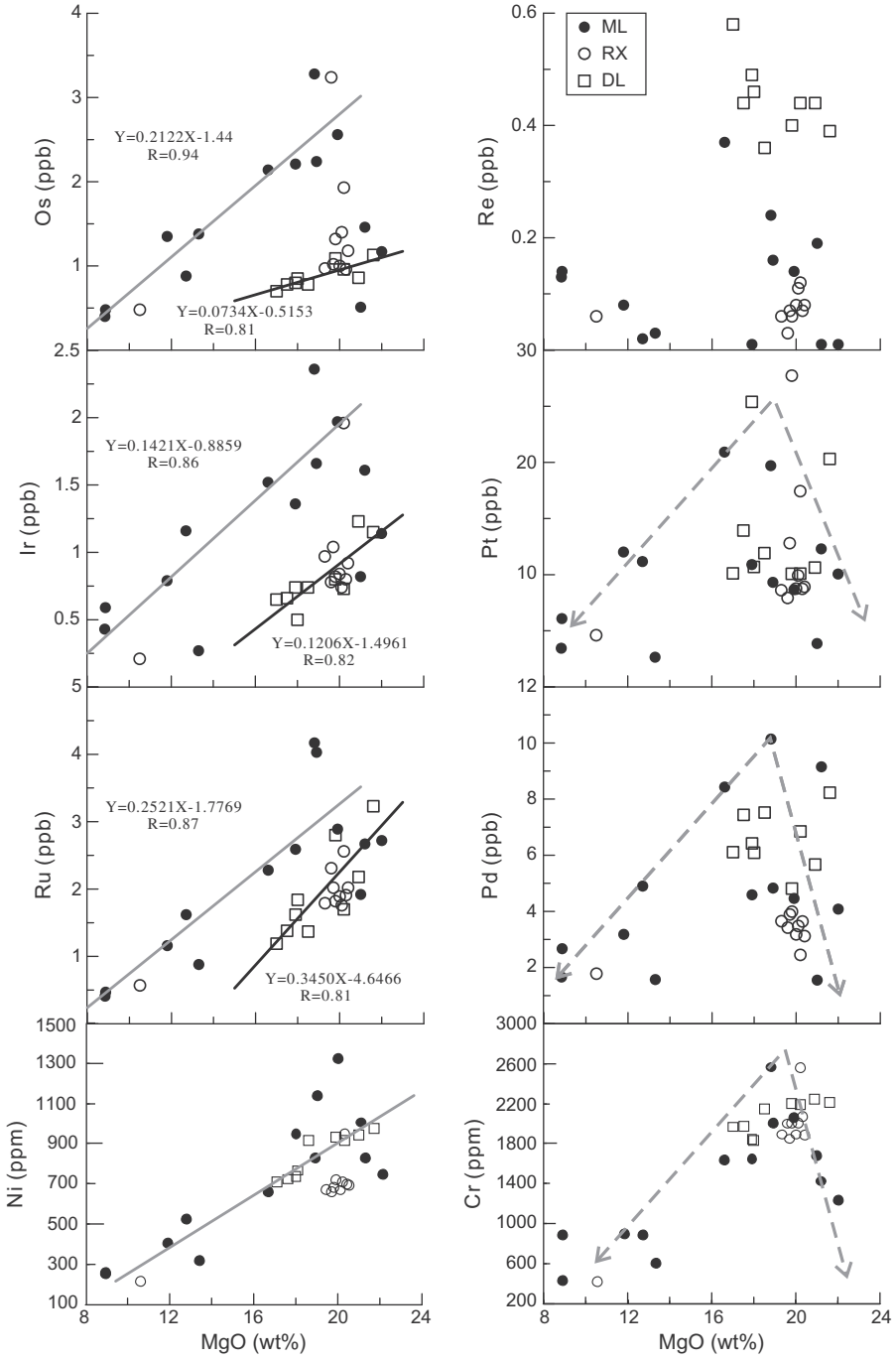

Fig. 5. PGE concentrations in the Muli and Dali picrites plotted versus MgO. Due to the narrow range of MgO contents in the Dali samples, the two picrite suites are shown separately on different plots.

display a linear correlation between Re and MgO, indicating that olivine fractionation and/or accumulation has had little effect on Re fractionation and concentrations. The Re concentration (0.25 ± 0.05 ppb) in the parental melts of the Muli picrites is derived from the average Re concentration for samples ML-28, ML04-20, ML04-45. Li et al. (2010) considered that these three samples were derived directly from the Emeishan mantle plume source with little or no lithospheric contamination.

In the Dali picrites, the DL samples defined good correlations between Os, Ir and Ru and MgO (Fig. 5). Osmium, Ir, and Ru contents of the DL parental melts were estimated as follows: Os = 0.88 ± 0.34 ppb, Ir = 0.80 ± 0.34 ppb, Ru = 1.90 ± 0.82 ppb. Platinum, Pd and Re do not display clear linear correlations with MgO in the DL suite, which indicates that olivine fractionation may have exerted little control on Pt, Pd and Re concentrations. The parental melt concentrations for these three elements can be constrained by the average of samples with MgO = 18–20 wt.% (Pt = 11.2 ± 1.5 ppb, Pd = 6.40 ± 0.97 ppb, Re = 0.45 ± 0.07 ppb). The RX samples do not display significant correlations between PGE concentrations and MgO content, perhaps due to their limited range and high values of MgO contents. PGE concentrations of the parental melts for the RX samples were constrained by the average values of these picrites (Os = 1.45 ± 0.74, Ir = 0.98 ± 0.38, Ru = 2.01 ± 0.26, Pt = 12.3 ± 6.5 and Pd = 3.42 ± 0.47 ppb).

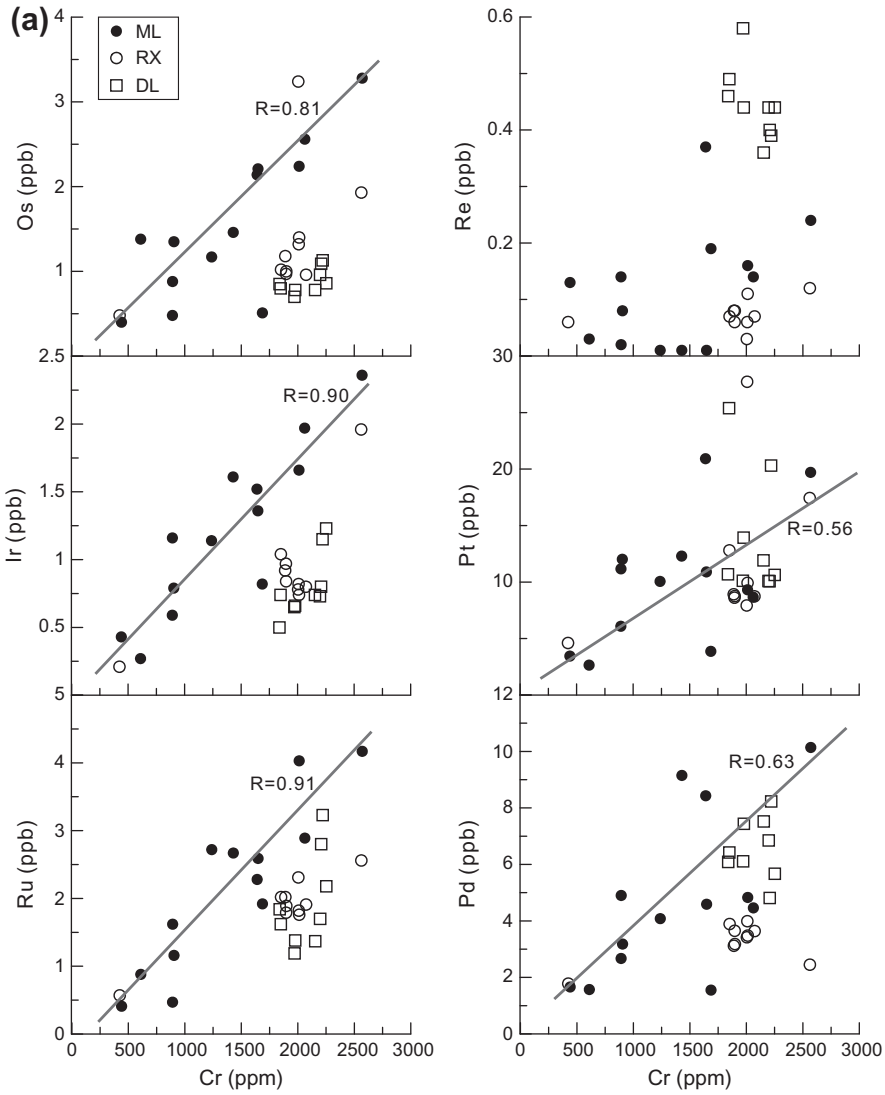

Fig. 6. PGE concentrations in Muli and Dali picrites plotted versus (a) Cr and (b) Ni contents.

The estimated HSE abundances of the parental melt for the Dali and Muli picrites are higher than the estimates for parental melts to Hawaiian picrites (Os = 0.50–1.0, Ir = 0.38–0.50, Ru = 2.20–2.55, Pt = 2.20–2.25, Pd = 2.20 and Re = 0.30–1.20 ppb; Ireland et al., 2009), and are consistent with previously published parental magma HSE concentrations for Emeishan picrites (Ir = 1.32, Ru = 1.96, Rh = 0.65, Pt = 5.79 and Pd = 7.93 ppb; Li et al., 2012).

5.4. Estimated bulk distribution coefficients

Linear regressions between PGE concentrations and MgO contents can be used to estimate bulk solid-melt partition coefficients (i.e., *D* values; Ireland et al., 2009; Puchtel and Humayun, 2001). Applying the same method proposed by Ireland et al. (2009), we estimated the bulk HSE concentrations in the co-precipitating solid phases. In the Muli and DL picrites, estimated D values for Os (3.4 and 3.6, respectively), Ir (4.0 and 4.3) and Ru (1.7 and 1.8) indicate that these elements all behaved compatibly. Our estimated D values are similar to those for Hawaiian picrites (e.g., D_{Os} = 2.2–7.1, Ireland et al., 2009). Platinum and Pd normally behave incompatibly in mafic to ultramafic systems in the absence of sulfides (e.g., Maier et al., 2009; Puchtel et al., 2009), whereas Pt and Pd display a complex behavior in our picrites samples (Fig. 5). At MgO $\leqslant$ 19 wt.%, Pt and Pd are generally positively correlated positively with MgO, indicating that these two elements were behaving compatibly. At MgO > 19 wt.%, Pt and Pd decrease with increasing MgO. These negative correlations may suggest that the PGE are hosted in chromite and sulfide inclusions present within the olivine grains, rather than structurally bound within the olivine lattice (e.g., Brenan et al., 2003, 2005; Ireland et al., 2009; Puchtel et al., 2001).

5.5. PGE and Re behavior during basalt petrogenesis

5.5.1. Lithosphere assimilation

Assimilation of lithosphere (crust and mantle) can also potentially affect the HSE characteristics and Os isotopic composition of a melt (e.g., Jamais et al., 2008). Assimilation of continental crust by the Emeishan CFBs has been suggested for highly evolved lavas from Guizhou (MgO < 8 wt.%) (Qi and Zhou, 2008). However, the Muli picrites with the most radiogenic Os isotope compositions also have high Os concentrations (>1.8 ppb) (Li et al., 2010). Mass balance calculations demonstrated that assimilation of ca. 50–60% crust would be required to produce the radiogenic Os of the Muli picrites (Li et al., 2010). However, this is inconsistent with the major element chemistry of the picrites. Addition of more

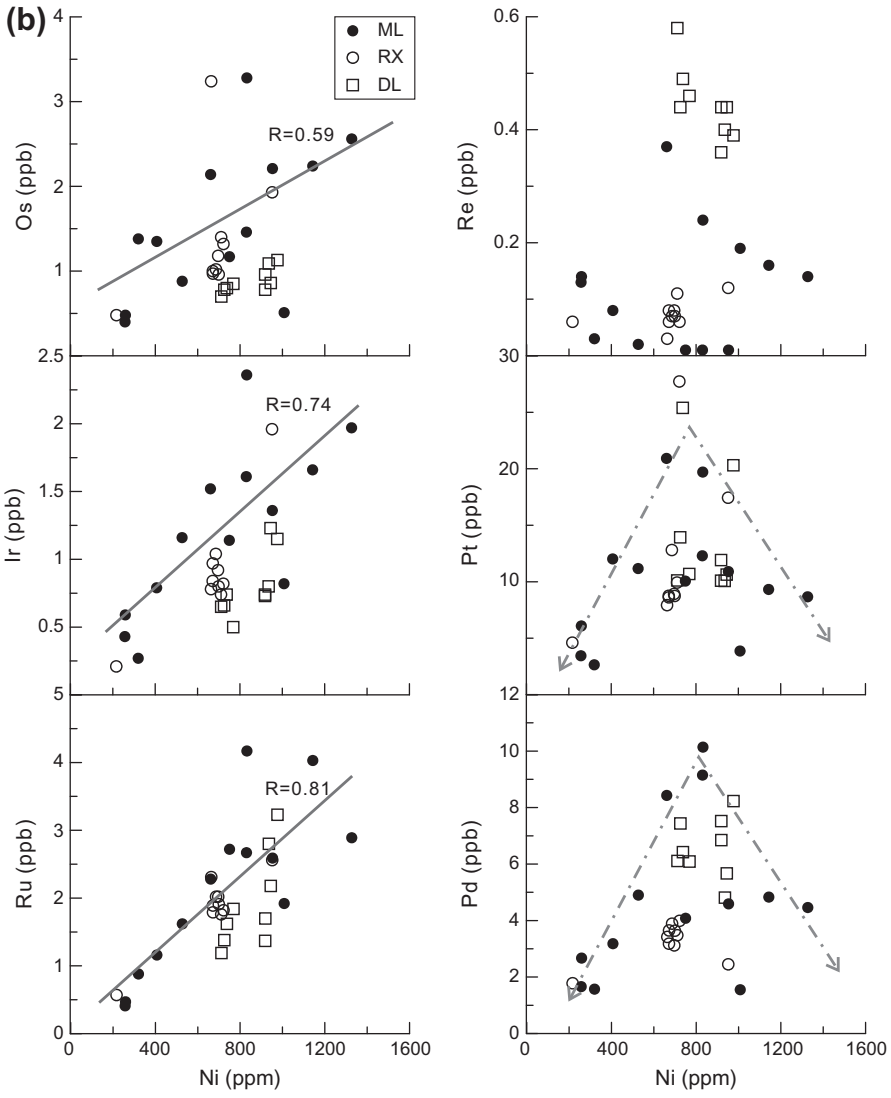

Fig. 6 (*continued*)

Table 4
Results of primary melt calculations using Herzberg modeling.

Sample	SiO_2	TiO_2	Al_2O_3	Cr_2O_3	Fe_2O_3	FeO	MnO	MgO	CaO	Na_2O	K_2O	NiO	P_2O_5
ML04-33	48.03	1.54	8.52	0.25	0.67	10.50	0.19	19.22	10.84	0.19	0.02	0.13	0.15
DL08-5	47.42	1.17	10.99	0.31	1.85	9.09	0.16	16.77	10.02	1.27	0.72	0.08	0.15
DL08-6	47.07	1.20	10.14	0.29	1.91	9.42	0.16	17.65	10.00	1.17	0.73	0.09	0.16
DL08-7	46.77	1.14	9.85	0.37	2.06	9.58	0.17	18.04	10.10	1.12	0.55	0.08	0.15
DL08-8	47.07	1.19	10.17	0.29	1.90	9.43	0.17	17.67	10.03	1.13	0.71	0.09	0.15
DL08-16	47.77	1.23	10.75	0.31	1.84	9.18	0.16	17.08	9.53	1.14	0.77	0.09	0.16

geologically realistic amounts of crust (<5%) would not result in resolvable variations of the HSE abundance. A hypothetical mixture of the Muli picrites, ingestion of 10% of upper continental crust component (0.02 ppb Os; $^{187}Os/^{188}Os = 0.8$, $\gamma_{Os} = +540$; Esser and Turekian, 1993) with 260 Ma picritic melts (1.2 ppb Os, $^{187}Os/^{188}Os = 0.1252$, and $\gamma_{Os} = 0$; Li et al., 2010) would result in a net change in the Os isotopic composition of the contaminated melt by only +0.9 γ unit. We therefore conclude that crustal contamination is unlikely to have significantly affected the HSE composition of our studied picrites.

Another mechanism to produce the observed HSE fractionations is silicate liquid immiscibility brought about by changes in the sulfur saturation state, and separation of an immiscible sulfur liquid and/or crystallization of sulfied minerals (Charlier et al., 2011). This requires that the highly magnesian volcanism was spatially and temporally associated with high-silica and high-iron melts (Jakobsen et al., 2005, 2011). However, the following lines of evidence rule out this possibility. Firstly, there are no high-silica igneous rocks spatially and temporally associated with the highly magnesium volcanism. Secondly, results from experimental studies that show that silicate liquid immiscibility in basaltic magma only starts at low temperatures and is limited to the final stages of magma crystallization (Jakobsen et al., 2011; references therein). In contrast, our studied samples are high-temperature and primitive magmas.

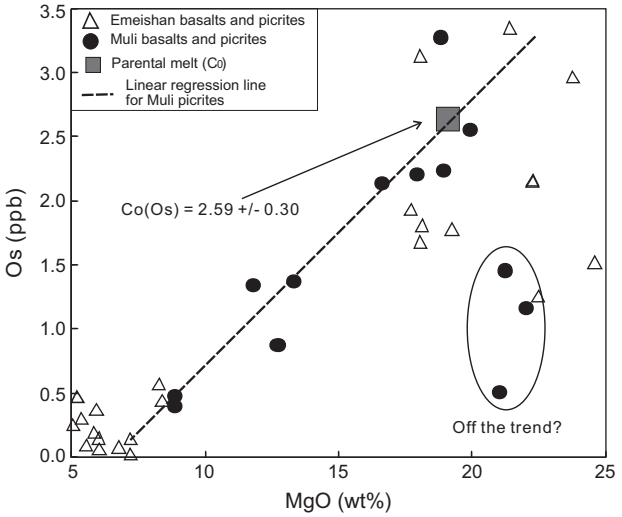

Fig. 7. Example of how the parental HSE melt contents were estimated using Os abundances from the Muli picrites. The parental melt was assumed to contain 19 wt.% MgO and its Os abundance was determined by linear regression through the data. Three samples do not plot on the regression trend.

Thirdly, the studied picrites defined a clear negative correlation between $Fe_2O_3^T$ and SiO_2 ($Fe_2O_3^T = -9.702 \times \ln(Fe_2O_3T) + 49.044$, $r^2 = 0.63$). This correlation is also inconsistent with the predicted effects of silicate liquid immiscibility.

Our currently available data cannot rule out assimilation of subcontinental lithospheric mantle during the ascent of the plume-derived melts through lithosphere. This is due to the fact that the Muli picrites have unradiogenic initial Os and Nd isotopic compositions with γOs (260 Ma) and εNd (260 Ma) values ranging from −4.2 to +11.5 and −5.5 to +6.4, respectively (Li et al., 2010).

5.5.2. Effects of partial melting and crystal-liquid fractionation

Partial melting is a potential controlling factor in producing HSE fractionations (e.g., Barnes et al., 1985; Shirey and Walker, 1998; Pearson et al., 2004; Ireland et al., 2009). The distinctive chondrite-normalized patterns, and relative and absolute contents of HSE are observed in different types of mantle-derived melts, such as some komatiites and typical MORB. Higher degree partial melts (>20%), such as some komatiites, have relatively flat chondrite-normalized HSE patterns that approach chondritic Pd/Ir ratios (Puchtel and Humayun, 2000, 2001; Puchtel et al., 2004; 2005). In contrast, low-degree partial melts, such as typical MORB, are generally characterized by fractionated chondrite-normalized HSE patterns

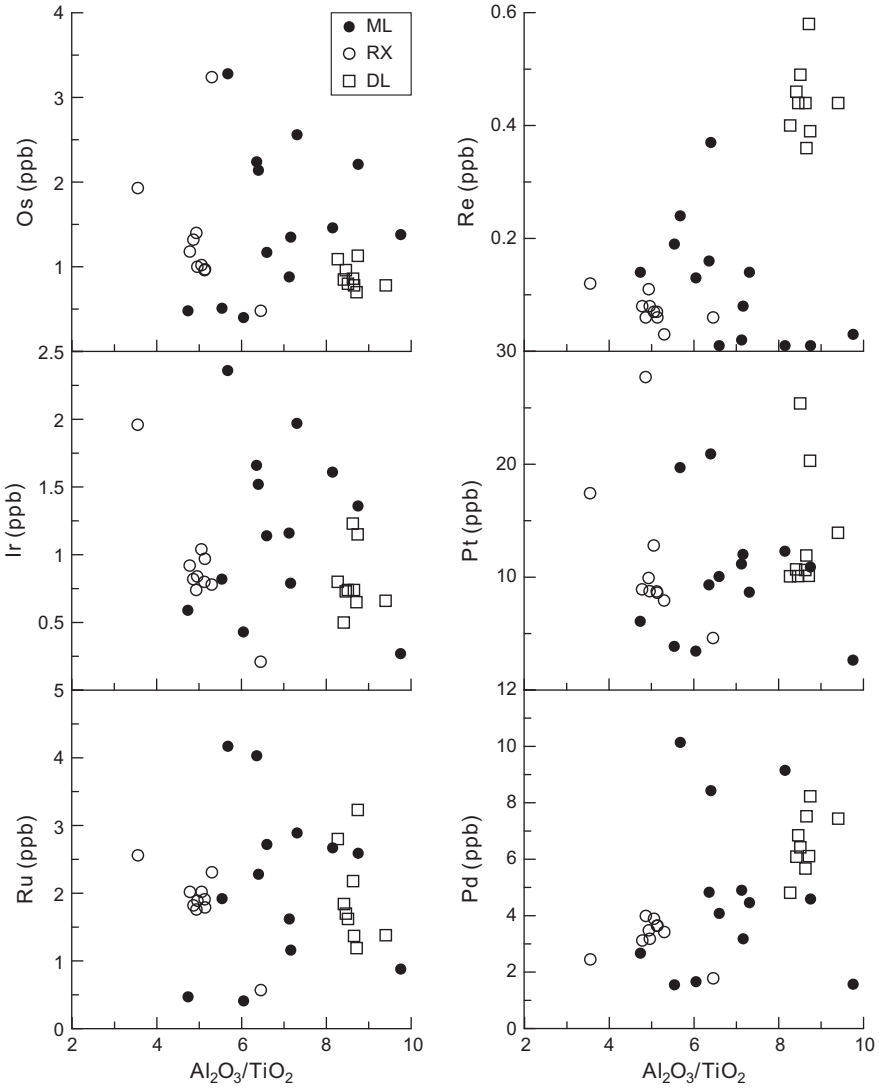

Fig. 8. PGE concentrations plotted versus Al_2O_3/TiO_2 ratios.

with high Pd/Ir and Pt/Ir ratios (Rehkamper et al., 1999; Bezos et al., 2005; Dale et al., 2008; Ireland et al., 2009).

Chondrite-normalized PGE patterns for the estimated Emeishan parental melts are comparable with those of komatiites and parental melts to Hawaiian picrites, which have been attributed to limited retention of I-PGE in their mantle sources due to saturation in Ir-(Os) alloys (e.g., Ireland et al., 2009; Fiorentini et al., 2011). Fractionation between I-PGE and P-PGE suggests the presence of residual sulfide in the plume source (Bennett et al., 2000).

The Muli and DL suite picrites exhibit positive correlations between I-PGE and MgO, Ni and Cr (Figs. 5 and 6). Although the RX samples do not show significant linear correlations, data for these samples largely fall on the trend defined by data for the DL picrites. This implies that early fractional crystallization of olivine, spinel and clinopyroxene is effective in removing the I-PGE from the magma. During the early stages of crystal fractionation, I-PGE may form laurite and Os–Ir–Ru alloys (e.g., Amosse et al., 1990; Capobianco and Drake, 1990; Qi and Zhou, 2008), which become trapped in early crystallizing phases, such as chromite and olivine (e.g., Puchtel and Humayun, 2000), and this effectively removes the I-PGE from the melt (Qi and Zhou, 2008).

The Muli picrites show a change in trends of Pt and Pd versus MgO diagram at MgO = ~19 wt.%. In plots of Pt and Pd versus Ni inflections also characterize the trends at Ni = 900 ppm. The Ni-MgO correlation in the Muli suite can be described by a regression where Ni (ppm) = 70.1 × MgO (wt.%) − 395. At MgO = 19 wt.%, this corresponds to Ni = 937 ppm for the parental melt. This suggests that the parental melts have the highest Pt and Pd values. The steep chondrite-normalized PGE patterns of the analyzed picrites clearly indicate fractionation between I-PGE and P-PGE (Fig. 3). A positive correlation between Os and Cr (Fig. 6) thus suggests that the PGE variations may be partially attributed to early fractionation of olivine (±chromite).

5.5.3. Source heterogeneities

Estimated PGE concentrations are highly variable in the primary melts of the Dali and Muli picrites. Due to the lack of systematic difference in partial melting processes in producing the Muli and Dali picrites, the large variations in absolute and relative HSE abundances most likely reflects source heterogeneity. Furthermore, the large range in Al_2O_3/TiO_2 and La/Yb ratios provides further evidence for source heterogeneity. Given that olivine fractionation or accumulation cannot fractionate these two ratios from their source values, the variations must reflect the crustal contamination and/or source heterogeneity. However, as crustal contamination was insignificant in generating the Dali and Muli picrites the large

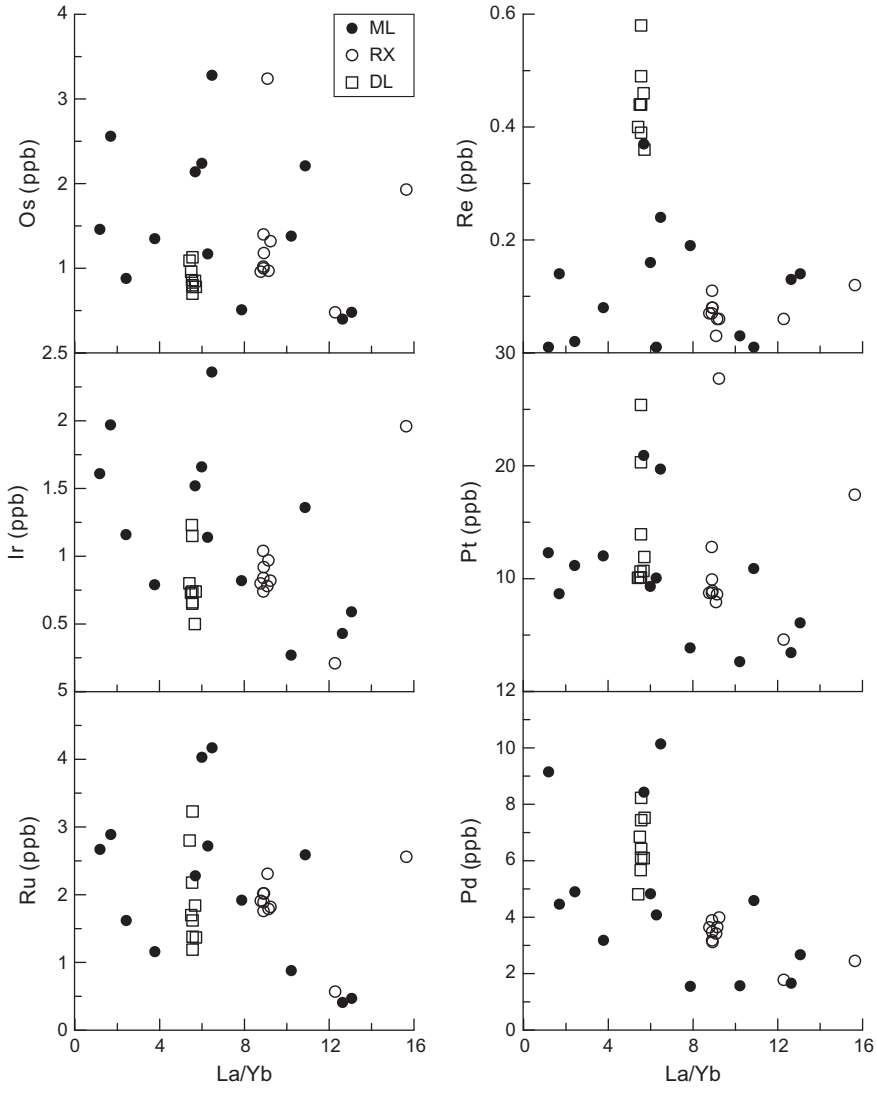

Fig. 9. PGE concentrations plotted versus La/Yb ratios.

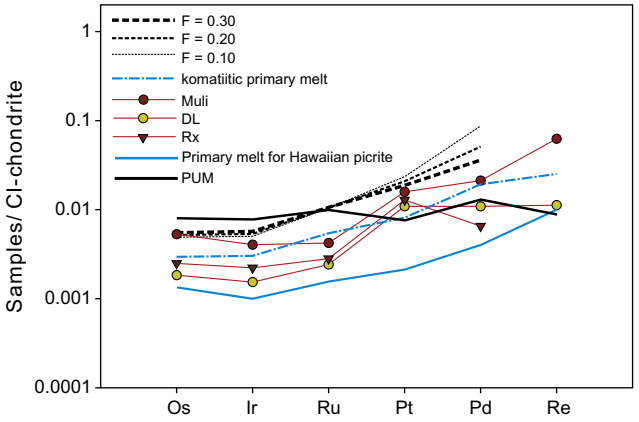

Fig. 10. Comparison of the estimated parental melts for the Muli, DL, and RX picrites with primary melts of the Hawaiian picrites (Ireland et al., 2009), komatiites (Puchtel and Humayun, 2000), PUM (Becker et al., 2006), and partial melts (black dashed lines) of a hybrid source comprising 99.9% primitive mantle and 0.1% outer core. The compositions of primitive mantle and outer core, and the bulk partition coefficients (D values), are from Puchtel and Humayun (2000). The normalizing values are from McDonough and Sun, 1995.

range in Al_2O_3/TiO_2 and La/Yb ratios suggests the Emeishan mantle plume was heterogeneous. The PGE contents in Muli picrites broadly correlate with Al_2O_3/TiO_2 and La/Yb ratios (apart from Re; Figs. 8 and 9), and, as such the PGE can be used to infer the source heterogeneity. This is consistent with Os–Nd–Sr isotope and elemental analyses of the Muli picrites (Li et al., 2010). Li et al., 2010 proposed that the generation of the Muli picrites involved at least three reservoirs, which were enriched and depleted plume source, and sub-continental lithospheric mantle. Plume-lithosphere interaction played an important role in producing the geochemical diversity of the Emeishan CFBs (e.g., Li et al., 2010; Xiao et al., 2004). The Muli picrites have a large range of initial Os isotopic compositions with γOs (260 Ma) = +11 to −5 (Li et al., 2010). These Os isotopic variations require long-term differences in the Re/Os ratios of the mantle sources. Previous studies have attributed the $^{187}Os/^{188}Os$ variations to the presence of recycled oceanic lithosphere and plume-lithosphere interaction (Li et al., 2010). The enrichment of ^{187}Os may reflect the contributions from a recycled oceanic lithospheric component or Earth's core (Li et al., 2010). Partial melting modeling shows that incorporation of a small proportion of outer core materials (ca. 0.1%) could explain the high PGE contents of the Muli picrites (Fig. 10). Other factors, such as the degree of partial melting, may also influence HSE concentrations, as a melt fraction which is just sufficient to exhaust sulfied in the source will produce a more HSE-rich melt than one resulting from a much higher degree of partial melting, where the HSE are further HSE-poorer melt. If this is correct, then correlations (and inflections) between HSE concentrations and La/Yb ratios in Fig. 9 are to be expected, because La/Yb ratios in a mafic to ultramafic magmas are directly related to the melt fraction. However, our data show no meaningful correlations between La/Yb and HSE concentrations and, as such we prefer the core-addition to explain the high HSE concentrations of the Emeishan picrites.

6. Conclusions

The Emeishan picrites are characterized by high absolute abundances of HSE. Chondrite -normalized HSE patterns of the picrites can be divided into two types: (a)Type-1, as represented by the Muli picrites, are similar to PUM with lower overall I-PGE abundances and lower relative and absolute Re abundances; (b) Type-2, as represented by the Dali picrites, are similar to those of East Greenland and Iceland picrites, which are characterized by more fractionated Pt/Ir (8.6–34.5; average = 15.9 ± 8.4) and Pd/Ir (1.3–12.1; average = 6.6 ± 3.0) ratios relative to Type-1 picrites.

We estimated the major element compositions of parental melts for the picrites using back-addition of equilibrium olivine into selected whole-rock compositions. The estimated primary melts of the picrites have MgO contents of ca. 18–19 wt.%. The effects of crystal-liquid fractionation processes are evident in plots of HSE abundances versus MgO. For those plots that show broad linear trends between HSE and MgO regression of these trends provides a means to estimate the HSE composition of the parental melts for each picritic suite. The HSE concentrations at MgO = 19 wt.% on these regressions were used to define the primary HSE abundances of the parental melts. However, the primary abundances of some elements that do not correlate with MgO were estimated by the average compositions of the samples that have MgO contents similar to those estimated for primary melts. Estimated HSE concentrations for the Muli picrites are Os = 2.59 ± 0.30, Ir = 1.84 ± 0.45, Ru = 3.00 ± 0.69, Pt = 16 ± 4, Pd = 10 ± 4, and Re = 0.25 ± 0.05 ppb (±2SD). The estimated HSE concentrations for the DL picrites from the Dali suite are Os = 0.88 ± 0.34, Ir = 0.80 ± 0.34, Ru = 1.90 ± 0.82. Pt = 11.2 ± 1.5, Pd = 6.40 ± 0.97, and Re = 0.45 ± 0.07 ppb. The RX samples do not display significant correlations between PGE concentrations and MgO content, and so the HSE contents of parental melts for the RX samples were constrained by the average PGE values of these primitive picrites (MgO = 20–21 wt.%). The obtained average values are Os = 1.45 ± 0.74, Ir = 0.98 ± 0.38, Ru = 2.01 ± 0.26, Pt = 12.3 ± 6.5, and Pd = 3.42 ± 0.47 ppb. The estimated parental melt HSE abundances for the Dali and Muli picrites are generally similar to, but higher than, estimates for parental melts of Hawaiian picrites.

The HSE display a large range of absolute and relative abundances in the Emeishan picrites. Detailed consideration of the PGE geochemistry shows that this reflects the integrated effects of source heterogeneity, partial melting, plume–lithosphere interaction, and early fractionation of olivine (±chromite). Our estimated HSE abundances for primary melts of the Emeishan picrites, combined with previously published isotopic data, provide new evidence that the Emeishan mantle plume was chemically heterogeneous.

Acknowledgements

E. Hanski is thanked for critical comments on an earlier version of this paper. Liu Yin and X.L. Tu are thanked for their assistance with major and trace element analyses. We are grateful to G. Shellnutt, E. Hanski and C. Dale for their constructive reviews. This study was jointly supported by the National Science Foundation of China (Grants 40903007, 41173038 and 41172064) and an Australian Research Council (ARC) ESTAR Fellowship through the ARC Centre of Excellence for Core to Crust Fluid Systems (CCFS). This is contribution No. IS- 1745 from GIG-CAS, and this is TIGeR publication No. 487 and CCFS contribution 347.

References

Ali, J.R., Thompson, G.M., Zhou, M.-F., Song, X., 2005. Emeishan large igneous province, SW China. Lithos 79, 475–489.

Amosse, J., Allibert, M., Fischer, W., Piboule, M., 1990. Experimental study of the solubility of platinum and iridium in basic silicate melts—implications for the differentiation of platinum-group elements during magmatic processes. Chem. Geol. 81, 45–53.

Anderson, D.L., Natland, J.H., 2005. A brief history of the plume hypothesis and its competitors: concepts and controversy. In: Foulger, G.R., Natland, J.H., Presnall, D.C., Anderson, D.L. (Eds.), Plates, Plumes, and Paradigms. Geological Society of America Special Paper 388, pp. 119–145.

Barnes, S.-J., Naldrett, A.J., Gorton, M.P., 1985. The origin of the fractionation of platinum-group elements in terrestrial magmas. Chem. Geol. 53, 303–323.
Becker, H., Horan, M.F., Walker, R.J., Gao, S., Lorand, J.P., Rudnick, R.L., 2006. Highly siderophile element composition of the Earth's primitive upper mantle: Constraints from new data on peridotite massifs and xenoliths. Geochim. Cosmochim. Acta 70, 4528–4550.
Bennett, V.C., Norman, M.D., Garcia, M.O., 2000. Rhenium and platinum group element abundances correlated with mantle source components in Hawaiian picrites: sulphides in the plume. Earth Planet. Sci. Lett. 183, 513–526.
Bezos, A., Lorand, J.P., Humler, E., Gros, M., 2005. Platinumgroup element systematics in mid-oceanic ridge basaltic glasses from the Pacific, Atlantic, and Indian Oceans. Geochim. Cosmochim. Acta 69, 2613–2627.
Boven, A., Pasteels, P., Punzalan, L.E., Liu, J., Luo, X., Zhang, W., Guo, Z., Hertogen, J., 2002. 40Ar/39Ar geochronological constraints on the age and evolution of the Permo-Triassic Emeishan volcanic province, southwest China. J. Asian Earth Sci. 20, 157–175.
Brandon, A.D., Walker, R.J., 2005. The debate over core-mantle interaction. Earth Planet. Sci. Lett. 232, 211–225.
Brandon, A.D., Norman, M.D., Walker, R.J., Morgan, J.W., 1999. 186Os-187Os systematics of Hawaiian picrites. Earth Planet. Sci. Lett. 174, 25–42.
Brenan, J.M., McDonough, W.F., Dalpé, C., 2003. Experimental constraints on the partitioning of rhenium and some platinum-group elements between olivine and silicate melt. Earth Planet. Sci. Lett. 212, 135–150.
Brenan, J.M., McDonough, W.F., Ash, R., 2005. An experimental study of the solubility and partitioning of iridium, osmium and gold between olivine and silicate melt. Earth Planet. Sci. Lett. 237, 855–872.
Bryan, S.E., Ernst, R.E., 2008. Revised definition of Large Igneous Provinces (LIPs). Earth-Sci. Rev. 86, 175–202.
Campbell, I.H., 2007. Testing the plume theory. Chem. Geol. 241, 153–176.
Campbell, I.H., Griffiths, R.W., 1990. Implications of mantle plume structure for the evolution of flood basalts. Earth Planet. Sci. Lett. 99, 79–93.
Capobianco, C.J., Drake, M.J., 1990. Partitioning of ruthenium, rhodium, and palladium between spinel and silicate melt and implications for platinum group element fractionation trends. Geochim. Cosmochim. Acta 54, 869–874.
Charlier, B., Namur, O., Toplis, M.J., Schiano, P., Cluzel, N., Higgins, M.D., Vander Auwera, J., 2011. Large-scale silicate liquid immiscibility during differentiation of tholeiitic basalt to granite and the origin of the Daly gap. Geology 39, 907–910.
Chazey Iii, W.J., Neal, C.R., 2005. Platinum-group element constraints on source composition and magma evolution of the Kerguelen Plateau using basalts from ODP Leg 183. Geochim. Cosmochim. Acta 69, 4685–4701.
Chen, J.L., Xu, J.F., Wang, B.D., Kang, Z.Q., Li, J., 2010. Origin of Cenozoic alkaline potassic volcanic rocks at KonglongXiang, Lhasa terrane, Tibetan Plateau: products of partial melting of a mafic lower-crustal source? Chem. Geol. 273, 286–299.
Chung, S.-L., Jahn, B.-m., 1995. Plume-lithosphere interaction in generation of the Emeishan flood basalts at the Permian–Triassic boundary. Geology 23, 889–892.
Coffin, M.F., Eldholm, O., 1992. Volcanism and continental break-up: a global compilation of large igneous provinces. Geological Society, vol. 68. Special Publications, London, pp. 17–30.
Cohen, A.S., Waters, G.G., 1996. Separation of osmium from geological materials by solvent extraction for analysis by thermal ionization mass spectrometry. Anal. Chim. Acta 332, 269–275.
Creaser, R.A., Papanastassiou, D.A., Wasserburg, G.J., 1991. Negative thermal ion mass spectrometry of osmium, rhenium and iridium. Geochim. Cosmochim. Acta 55, 397–401.
Dale, C.W., Luguet, A., Macpherson, C.G., Pearson, D.G., Hickey-Vargas, R., 2008. Extreme platinum-group element fractionation and variable Os isotope compositions in Philippine Sea Plate basalts: tracing mantle source heterogeneity. Chem. Geol. 248, 213–238.
Danyushevsky, L.V., Della-Pasqua, F.N., Sokolov, S., 2000. Re-equilibration of melt inclusions trapped by magnesian olivine phenocrysts from subduction-related magmas: petrological implications. Contrib. Mineral. Petrol. 138, 68–83.
Ely, J.C., Neal, C.R., 2003. Using platinum-group elements to investigate the origin of the Ontong Java Plateau, SW Pacific. Chem. Geol. 196, 235–257.
Esser, B.K., Turekian, K.K., 1993. The osmium isotopic composition of the continental crust. Geochim. Cosmochim. Acta 57, 3093–3104.
Fan, W.M., Zhang, C.H., Wang, Y.J., Guo, F., Peng, T.P., 2008. Geochronology and geochemistry of Permian basalts in western Guangxi Province, Southwest China: evidence for plume-lithosphere interaction. Lithos 102, 218–236.
Fiorentini, M.L., Barnes, S.J., Maier, W.D., Burnham, O.M., Heggie, G., 2011. Global variability in the platinum-group element contents of komatiites. J. Petrol. 52, 83–112.
Foulger, G.R., Natland, J.H., Presnall, D.C., Anderson, D.L. (Eds.), 2005. Plates, Plumes, and Paradigms. Geological Society of America Special Paper 388, pp. 881.
Frost, D.J., McCammon, C.A., 2008. The redox state of Earth's mantle. Ann. Rev. Earth Planet. Sci. 36, 389–420.
Hanski, E., Walker, R.J., Huhma, H., Polyakov, G.V., Balykin, P.A., Hoa, T.T., Phuong, N.T., 2004. Origin of Permian–Triassic komatiites, northwestern Vietnam. Contrib. Mineral. Petrol. 147, 453–469.
Hanski, E., Kamenetsky, V.S., Luo, Z.-Y., Xu, Y.-G., Kuzmin, D.V., 2010. Primitive magmas in the Emeishan large igneous province, southwestern China and northern Vietnam. Lithos 119, 75–90.
He, B., Xu, Y., Xiao, L., Chung, S., Wang, Y., 2003. Sedimentary evidence for a rapid, kilometer-scale crustal doming prior to the eruption of the Emeishan flood basalts. Earth Planet. Sci. Lett. 213, 391–405.
He, B., Xu, Y.G., Huang, X.L., Luo, Z.Y., Shi, Y.R., Yang, Q.J., Yu, S.Y., 2007. Age and duration of the Emeishan flood volcanism, SW China: Geochemistry and SHRIMP zircon U-Pb dating of silicic ignimbrites, post-volcanic. Earth Planet. Sci. Lett. 255, 306–323.
Herzberg, C., Gazel, E., 2009. Petrological evidence for secular cooling in mantle plumes. Nature 458, 619–622.
Herzberg, C., Asimow, P.D., Arndt, N., Niu, Y., Lesher, C.M., Fitton, J.G., Saunders, A.D., 2007. Temperature in ambient mantle and plumes: constraints from basalts, picrites, and komatiites. Geochem. Geophys. Geosyst. 8. http://dx.doi.org/10.1029/2006GC001390.
Ireland, T.J., Walker, R.J., Garcia, M.O., 2009. Highly siderophile element and 187Os isotope systematics of Hawaiian picrites: Implications for parental melt composition and source heterogeneity. Chem. Geol. 260, 112–128.
Ireland, T.J., Walker, R.J., Brandon, A.D., 2011. 186Os-187Os systematics of Hawaiian picrites revisited: new insights into Os isotopic variations in ocean island basalts. Geochim. Cosmochim. Acta 75, 4456–4475.
Jakobsen, J.K., Veksler, I.V., Tegner, C., Brooks, C.K., 2005. Immiscible iron- and silica-rich melts in basalt petrogenesis documented in the Skaergaard intrusion. Geology 33, 885–888.
Jakobsen, J.K., Veksler, I.V., Tegner, C., Brooks, C.K., 2011. Crystallization of the Skaergaard Intrusion from an Emulsion of Immiscible Iron- and Silica-rich Liquids: Evidence from Melt Inclusions in Plagioclase. J. Petrol. 52, 345–373.
Jamais, M., Lassiter, J.C., Brügmann, G., 2008. PGE and Os-isotopic variations in lavas from Kohala Volcano, Hawaii: constraints on PGE behavior and melt/crust interaction. Chem. Geol. 250, 16–28.
Lassiter, J.C., 2003. Rhenium volatility in subaerial lavas: constraints from subaerial and submarine portions of the HSDP-2 Mauna Kea drillcore. Earth Planet. Sci. Lett. 214, 311–325.
Li, J., Xu, J.-F., Suzuki, K., He, B., Xu, Y.-G., Ren, Z.-Y., 2010. Os, Nd and Sr isotope and trace element geochemistry of the Muli picrites: Insights into the mantle source of the Emeishan large igneous province. Lithos 119, 108–122.
Li, C., Yan, T., Qi, L., Ripley, E.M., 2012. Controls on PGE fractionation in the Emeishan picrites and basalts: Constraints from integrated lithophile–siderophile elements and Sr–Nd isotopes. Geochim. Cosmochim. Acta 90, 12–32.
Li, J., Jiang, X.-Y., Xu, J.-F., Zhong, L.-F., Wang, X.-C., Wang, G.-Q., Zhao, P.-P., in press. Determination of Platinum-Group Elements and Re-Os Isotopes using ID-ICP-MS and N-TIMS from a Single Digestion after Two-Stage Column Separation. Geostand. Geoanal. Res..
Lo, C.H., Chung, S.L., Lee, T.Y., Wu, G.Y., 2002. Age of the Emeishan flood magmatism and relations to Permian–Triassic boundary events. Earth Planet. Sci. Lett. 198, 449–458.
Maier, W.D., Barnes, S.J., Campbell, I.H., Fiorentini, M.L., Peltonen, P., Barnes, S.-J., Smithies, R.H., 2009. Progressive mixing of meteoritic veneer into the early Earth's deep mantle. Nature 460, 620–623.
McDonough, W.F., Sun, S.s., 1995. The composition of the Earth. Chem. Geol. 120, 223–253.
McHone, J.G., 2000. Non-plume magmatism and rifting during the opening of the central Atlantic Ocean. Tectonophysics 316, 287–296.
Meisel, T., Moser, J., 2004. Reference materials for geochemical PGE analysis: New analytical data for Ru, Rh, Pd, Os, Ir, Pt and Re by isotope dilution ICP-MS in 11 geological reference materials. Chem. Geol. 208, 319–338.
Meisel, T., Moser, J., Kettisch, P., 2008. Determination of Osmium and Other Platinum Group Elements in Chromitites by Acid Digestion and ICPMS. Department of General and Analytical Chemistry, University of Leoben, Leoben, pp. 1.
Momme, P., Tegner, C., Brooks, K., Keays, R., 1997. The behaviour of platinum-group elements in basalts from the East Greenland rifted margin. Contrib. Mineral. Petrol. 143, 133–153.
Momme, P., Óskarsson, N., amp, x, els, Keays, R.R., 2003. Platinum-group elements in the Icelandic rift system: melting processes and mantle sources beneath Iceland. Chem. Geol. 196, 209–234.
Momme, P., Tegner, C., Brooks, C.K., Keays, R.R., 2006. Two melting regimes during Paleogene flood basalt generation in East Greenland: combined REE and PGE modelling. Contrib. Mineral. Petrol. 151, 88–100.
Norman, M.D., Garcia, M.O., Bennett, V.C., 2004. Rhenium and chalcophile elements in basaltic glasses from Ko'olau and Moloka'i volcanoes: magmatic outgassing and composition of the Hawaiian plume. Geochim. Cosmochim. Acta 68, 3761–3777.
Pearson, D.G., Irvine, G.J., Ionov, D.A., Boyd, F.R., Dreibus, G.E., 2004. Re-Os isotope systematics and platinum group element fractionation during mantle melt extraction: a study of massif and xenolith peridotite suites. Chem. Geol. 208, 29–59.
Pitcher, L., Helz, R.T., Walker, R.J., Piccoli, P., 2009. Fractionation of the platinum-group elments and Re during crystallization of basalt in Kilauea Iki Lava Lake, Hawaii. Chem. Geol. 260, 196–210.
Polat, A., Hoffmann, A.W., 2003. Alteration and geochemical patterns in the 3.7-3.8 Ga Isua greenstone belt. West Greenland. Precambrian. Res. 126, 197–218.
Puchtel, I., Humayun, M., 2000. Platinum group elements in Kostomuksha komatiites and basalts: implications for oceanic crust recycling and core-mantle interaction. Geochim. Cosmochim. Acta 64, 4227–4242.
Puchtel, I.S., Humayun, M., 2001. Platinum group element fractionation in a komatiitic basalt lava lake. Geochim. Cosmochim. Acta 65, 2979–2993.
Puchtel, I.S., Humayun, M., 2005. Highly siderophile element geochemistry of 187Os-enriched 2.8 Ga Kostomuksha komatiites, Baltic Shield. Geochim. Cosmochim. Acta 69, 1607–1618.

Puchtel, I.S., Brugmann, G.E., Hofmann, A.W., 2001. 187Os-enriched domain in an Archean mantle plume: evidence from 2.8 Ga komatiites of the Kostomuksha greenstone belt, NW Baltic Shield. Earth Planet. Sci. Lett. 186, 513–526.
Puchtel, I.S., Humayun, M., Campbell, A.J., Sproule, R.A., Lesher, C.M., 2004. Platinum group element geochemistry of komatiites from the Alexo and Pyke Hill areas, Ontario, Canada. Geochim. Cosmochim. Acta 68, 1361–1383.
Puchtel, I.S., Walker, R.J., Anhaeusser, C.R., Gruau, G., 2009. Re-Os isotope systematics and HSE abundances of the 3.5 Ga Schapenburg komatiites, South Africa: Hydrous melting or prolonged survival of primordial heterogeneities in the mantle? Chem. Geol. 262, 355–369.
Putirka, K.D., 2005. Mantle potential temperatures at Hawaii, Iceland, and the mid-ocean ridge system, as inferred from olivine phenocrysts: evidence for thermally driven mantle plume. Geochem. Geophys. Geosyst. 6, Q05L08, 1029/2005GC00091.
Putirka, K.D., Perfit, M., Ryerson, F.J., Jackson, M.G., 2007. Ambient and excess mantle temperatures, olivine thermometry, and active vs. passive upwelling. Chem. Geol. 241, 177–206.
Qi, L., Zhou, M.-F., 2008. Platinum-group elemental and Sr–Nd–Os isotopic geochemistry of Permian Emeishan flood basalts in Guizhou Province, SW China. Chem. Geol. 248, 83–103.
Rehkamper, M., Halliday, A.N., Fitton, J.G., Lee, D.C., Wieneke, M., Arndt, N.T., 1999. Ir, Ru, Pt, and Pd in basalts and komatiites: new constraints for the geochemical behavior of the platinum-group elements in the mantle. Geochim. Cosmochim. Acta 63, 3915–3934.
Richards, M.A., Duncan, R.A., Courtillot, V.E., 1989. Flood basalts and hot-spot tracks: plume heads and tails. Science 246, 103–107.
Righter, K., Campbell, A.J., Humayun, M., Hervig, R.L., 2004. Partitioning of Ru, Rh, Pd, Re, Ir, and Au between Cr-bearing spinel, olivine, pyroxene and silicate melts. Geochim. Cosmochim. Acta 68, 867–880.
Shellnutt, J.G., Jahn, B.-M., 2011. Origin of Late Permian Emeishan basaltic rocks from the Panxi region (SW China): implications for the Ti-classification and spatial-compositional distribution of the Emeishan basalts. J. Volcanol. Geotherm. Res. 199, 85–95.
Shellnutt, J.G., Denyszyn, S., Mundil, R., 2012. Precise age determination of mafic and felsic intrusive rocks from the Permian Emeishan large igneous province (SW China). Gondwana Res. 22, 118–126.
Shirey, S.B., Walker, R.J., 1995. Carius tube digestion for low-blank rhenium-osmium analysis. Anal. Chem. 67, 2136–2141.
Shirey, S.B., Walker, R.J., 1998. The Re-Os Isotope system in cosmochemistry and high-temeprature geochemistry. Ann. Rev. Earth Planet. Sci. 26, 423–500.
Song, X.-Y., Qi, H.-W., Robinson, P.T., Zhou, M.-F., Cao, Z.-M., Chen, L.-M., 2008. Melting of the subcontinental lithospheric mantle by the Emeishan mantle plume; evidence from the basal alkaline basalts in Dongchuan, Yunnan, Southwestern China. Lithos 100, 93–111.
Sun, W., Bennett, V.C., Eggins, S.M., Kamenetsky, V.S., Arculus, R.J., 2003. Enhanced mantle-to-crust rhenium transfer in undegassed arc magmas. Nature 422, 294–297.
Sun, Y. et al., 2010. Dating and onset and nature of the Middle Permian Emeishan large igneous province eruptions in SW China using conodont biostratigraphy and its bearing on mantle plume uplift models. Lithos 119, 20–33.
Utskins-Peate, I., Bryan, S.E., 2008. Re-evaluating plume induced uplift in the Emeishan large igneous province. Nat. Geosci. 1, 625–629.
Volkening, J., Walczyk, T.G., Heumann, K., 1991. Osmium isotope ratio determinations by negative thermal ionization mass spectrometry. Int. J. Mass Spectrom. Ion Pros. 105, 147–159.
Walker, D., 2000. Core participation in mantle geochemistry: geochemical society ingerson lecture, GSA Denver, October 1999. Geochim. Cosmochim. Acta 64, 2897–2911.
Walker, R.J., Morgan, J.W., Horan, M.F., 1995. Osmium-187 enrichment in some plumes: evidence for core-mantle interaction? Science 269, 819–822.
Wang, C.Y., Zhou, M.-F., Qi, L., 2007a. Permian flood basalts and mafic intrusions in the Jinping (SW China)–Song Da (northern Vietnam) district: Mantle sources, crustal contamination and sulfide segregation. Chem. Geol. 243, 317–343.
Wang, X.-C., Li, X.-H., Li, W.-X., Li, Z.-X., 2007b. Ca. 825 Ma komatiitic basalts in South China: first evidence for >1500 °C mantle melts by a Rodinian mantle plume. Geology 35, 1103–1106.
Wang, C., Zhou, M.-F., Qi, L., 2011. Chalcophile element geochemistry and petrogenesis of high-Ti and low-Ti magmas in the Permian Emeishan large igneous province, SW China. Contrib. Mineral Petrol. 161, 237–254.
Wang, X.-C., Li, Z.-X., Li, X.-H., Li, J., Liu, Y., Long, W.-G., Zhou, J.-B., Wang, F., 2012. Temperature, Pressure, and composition of the mantle source region of late Cenozoic Basalts in Hainan Island, SE Asia: a consequence of a young thermal mantle plume close to subduction zones? J. Petrol. 53, 177–233.
Xiao, L., Xu, Y.G., Mei, H.J., Zheng, Y.F., He, B., Pirajno, F., 2004. Distinct mantle sources of low-Ti and high-Ti basalts from the western Emeishan large igneous province, SW China: implications for plume-lithosphere interaction. Earth Planet. Sci. Lett. 228, 525–546.
Xu, Y., Chung, S.-L., Jahn, B.-m., Wu, G., 2001. Petrologic and geochemical constraints on the petrogenesis of Permian–Triassic Emeishan flood basalts in southwestern China. Lithos 58, 145–168.
Xu, Y.-G., He, B., Chung, S.-L., Menzies, M.A., Frey, F.A., 2004. Geologic, geochemical, and geophysical consequences of plume involvement in the Emeishan flood-basalt province. Geology 32, 917–920.
Zhang, Z., Mahoney, J.J., Mao, J., Wang, F., 2006. Geochemistry of Picritic and Associated Basalt Flows of the Western Emeishan Flood Basalt Province, China. J. Petrol. 47, 1997–2019.
Zhang, Z., Zhi, X., Chen, L., Saunders, A.D., Reichow, M.K., 2008. Re-Os isotopic compositions of picrites from the Emeishan flood basalt province, China. Earth Planet. Sci. Lett. 276, 30–39.
Zhang, Z., Mao, J., Saunders, A.D., Ai, Y., Li, Y., Zhao, L., 2009. Petrogenetic modeling of three mafic–ultramafic layered intrusions in the Emeishan large igneous province, SW China, based on isotopic and bulk chemical constraints. Lithos 113, 369–392.
Zhong, H., Zhu, W.G., 2006. Geochronology of layered mafic intrusions from the Pan-Xi area in the Emeishan large igneous province, SW China. Miner. Deposita 41, 599–606.
Zhong, H., Qi, L., Hu, R.-Z., Zhou, M.-F., Gou, T.-Z., Zhu, W.-G., Liu, B.-G., Chu, Z.-Y., 2011. Rhenium-osmium isotope and platinum-group elements in the Xinjie layered intrusion, SW China: Implications for source mantle composition, mantle evolution, PGE fractionation and mineralization. Geochim. Cosmochim. Acta 75, 1621–1641.
Zhou, M.F., Malpas, J., Song, X.Y., Robinson, P.T., Sun, M., Kenned, y, A.K., Lesher, C.M., Keays, R.R., 2002. A temporal link between the Emeishan large igneous province (SW China) and the end-Guadalupian mass extinction. Earth Planet. Sci. Lett. 196, 113–122.
Zhou, M.F., Arndt, N.T., Malpas, J., Wang, C.Y., Kennedy, A.K., 2008. Two magma series and associated ore deposit types in the Permian Emeishan large igneous province, SW China. Lithos 103, 352–368.